The Pennsylvania State University

The Graduate School

CONSTRAINTS FROM MONAZITE PETROCHRONOLOGY ON THE ASSEMBLY OF THE IVREA-VERBANO ZONE

A Thesis in

Geosciences

by

Damaris Wyatt

© 2019 Damaris Wyatt

Submitted in Partial Fulfillment
of the Requirements
for the Degree of

Master of Science

December 2019

The thesis of Damaris Wyatt was reviewed and approved* by the following:

Andrew Smye
Assistant Professor of Geosciences
Thesis Advisor

Kevin Furlong
Professor of Geosciences

Tanya Furman
Professor of Geosciences

Mark Patzkowsky
Professor and Associate Head for Graduate Programs and Research

*Signatures are on file in the Graduate School

ABSTRACT

The Ivrea-Verbano Zone (IVZ) in northwest Italy is an archetypal section of lower continental crust. This section is dominated by metasedimentary rocks, in contrast to constraints from geochemical data, seismic wave speeds, and heat flow estimates interpreted to reflect a mafic lower continental crustal composition. How, then, are sediments incorporated into lower continental crust? Burial, crustal underthrusting, and relamination are three tectonic mechanisms that could emplace sediments at lower crustal depths. This investigation seeks to constrain the prograde pressure-temperature-time (*P*-*T*-*t*) path of IVZ metapelites and compare it to the expected prograde *P*-*T*-*t* path for each mechanism to determine which is responsible for the assembly of the lower crustal section. The tectonic mechanisms are further assessed by comparing their predicted petrological and field scale characteristics with features observed in IVZ rocks. Laser ablation split stream (LASS) ICP-MS measurements of U-Pb dates and trace element concentrations in monazite grains found in two suites of amphibolite to granulite facies metapelitic rocks from Val Strona di Omegna, IVZ, provide a record of the Permian-to-Jurassic metamorphic history of the lower crust of the Southern Alpine basement. Monazite dates are quantitatively linked to P-T conditions through phase equilibria calculations and the yttrium-in-garnet and monazite (Y-MG) thermometer applied to the pre-300 Ma monazite population. These constraints on the prograde *P*-*T*-*t* evolution of the Ivrea Zone, combined with field and petrographic observations of IVZ metapelites, indicate that the IVZ lower crustal section likely formed through crustal underthrusting.

TABLE OF CONTENTS

LIST OF FIGURES

LIST OF TABLES

ACKNOWLEDGEMENTS

I would like to thank my advisor, Andy, for his endless patience and boundless enthusiasm. It has been an honor to be Andy's first student, and we learned together every step of the way. I would also like to thank my committee members Tanya Furman and Kevin Furlong for all the advice they shared with me, from the scientific to the practical.

This thesis was made possible by the Penn State Materials Characterization Laboratory, and I am so appreciative of all the knowledge and expertise that Kat Crispin, Julie Anderson, Wes Auker, Manuel Villalpando, and Teague Williams were willing to share with me. Many thanks to Andrew Kylander Clark of the UC Santa Barbara Laser-Ablation Split-Stream Lab for trusting me enough to let me use the LASS and for fielding my frantic late-night calls while using the machine.

Thank you to my group mates, field assistants and friends Dr. Joshua Garber and Jacob Cipar, for celebrating and/or commiserating with me whenever I needed it. I also thank my family and the entire PSU Geosciences community for all their love and support.

This project was funded in part by the P.D. Krynine Memorial Fund and the Charles E. Knopf, Sr., Memorial Scholarship.

Chapter 1

Introduction

Continental crust comprises ~40 % of the Earth's surface and is characterized by major compositional differences from oceanic crust (57-66 wt.% SiO_2, compared to 48-52 wt.% SiO_2; e.g., Rudnick & Gao 2003, 2014). While the formation and evolution of the uppermost continental crust (≤15-20 km) is well constrained due to its accessibility for direct investigation, the genesis of lower continental crust (≥20-25 km) is more obscure. Understanding the process of lower crustal assembly is relevant to geodynamics, geochemistry and seismology because the tectonic mechanisms that form lower continental crust impart observed seismic wave speed, compositional and heat flow characteristics. Determining the distribution of heat producing elements in the lower crust, for example, is important for understanding the strength distribution of the continental crust and could help address how large-scale continental rifting initiates and why some continental crust forms cratons that can preserve rocks for billions of years (Sandiford and McLaren 2002, Mareschal and Jaupart 2013). Seismically, determining the composition of the lower continental crust can allow for improved velocity models and resultant constraints on the structure of the lithosphere (Christensen and Mooney 1995).

Observations of the lower continental crust are limited to indirect sources like heat flow measurements and geophysical data, as well as direct sources like exposed metamorphic terrains, inferred to have equilibrated at lower crustal depths, and xenoliths that sample a range of crustal to mantle levels (Rudnick and Goldstein 1990, Rudnick and Fountain 1995, Hacker, Kelemen, and Behn 2015, Rudnick and Gao 2014). The current consensus is that continental lower crust is predominately mafic in composition. Rudnick & Gao (2003, 2014) estimated that ~80 % of

continental lower crust is mafic based on the compositions of lower crustal xenoliths and of granulite-facies terrains, the inferred heat flow from lower crust, and seismic wavespeeds, but more recent analyses reveal that these same constraints also allow for the lower crust to be dominated by felsic rocks (Hacker, Kelemen, and Behn 2011, 2015). Using heat flow estimates to determine lower crustal composition requires using values for composition and thickness of other crustal levels and inferred mantle heat flow that are not fully constrained (Rudnick and Gao 2003, Hacker, Kelemen, and Behn 2011, 2015). Seismic wave speeds can be related to rock density and SiO_2 content, but measuring P- and S-wave velocities at middle-to-lower crustal levels is imprecise and compositional estimates are based on the assumption that the lower crust is igneous (Hacker, Kelemen, and Behn 2015, Behn and Kelemen 2003). Lower crustal compositions ranging from 80% to 0% mafic can satisfy all the indirect observations depending on the assumptions made about thickness of lower continental crust, characteristics of middle and upper continental crust, mantle heat flow, and the behavior of seismic waves at depth (Rudnick and Gao 2003, Hacker, Kelemen, and Behn 2011).

Direct observations from crustal xenoliths and metamorphic terranes avoid the uncertainties and generalizations associated with indirect observations. They also reveal significant heterogeneity in the composition of the lower continental crust: amphibolite and granulite facies terrains and granulite facies xenoliths contain between 35 to 90 wt.% SiO_2, and bulk rock compositions indicate that 57-61% of metamorphic terrains and 25% of xenoliths have sedimentary protoliths (Hacker, Kelemen, and Behn 2015). Protoliths of metasediments in lower crustal xenoliths and exhumed high-grade terranes must have been originally deposited at the Earth's surface, but underwent subsequent metamorphism at depths of 25-40 km. This poses the question: *how are sediments incorporated into lower continental crust?*

We address this question with a field-based investigation of the prograde pressure-temperature-time evolution of an archetypal section of metasedimentary lower crust—the Ivrea-

Verbano Zone (IVZ), NW Italy. The IVZ offers the potential to directly study the deepest levels of the crust (Burke and Fountain 1990, Zingg et al. 1990, Quick, Sinigoi, and Mayer 1995, Sinigoi et al. 1996, Boriani and Villa 1997, Handy et al. 1999). A total of 14 kilometers of mid-to-lower crustal rocks are exposed in the IVZ, and the presence of ultramafic rocks at the base of the IVZ section indicates that the deepest structural levels were once juxtaposed with the Moho (Voshage et al. 1990). The IVZ is dominated by amphibolite to granulite facies metapelites and reached peak pressures and temperatures of ~10–12 kbar and 900–950°C at the base of the section, corresponding to depths of up to 38 km (Redler et al. 2012).

Chapter 2

Incorporation of sediments into lower crust

There are three tectonic mechanisms that could incorporate sediment into the lower continental crust: burial of sediments under continued deposition and volcanism, crustal underthrusting during continental collision, and relamination of viscous sediments from the down-going plate in a subduction zone setting.

In the burial mechanism (Fig. 2-1a), sediments are forced downwards into the lower crust by continual deposition of sedimentary and volcanic rocks from the surface (Lakatos and Miller 1983, Johnsson 1986, Liu, Bohlen, and Ernst 1996, Sakaguchi 1999). The *P-T-t* path of burial models is characterized by peak pressures that increases along a lithostatic gradient determined by the density of overlying sediments and volcanic material, and peak temperatures that increase downward along an equilibrium geothermal gradient reflecting steady state radiogenic heating and conductive heat loss (Fig. 2-2a) (Huerta, Royden, and Hodges 1998).

Crustal underthrusting (Fig. 2-1b) drives one tectonic plate beneath another plate during continental collision and the down-going plate becomes the *de facto* lower crust (Xu et al. 2015). Initial stages of the *P-T-t* path of the crustal underthrusting model follow a subduction zone type thermal gradient where pressure increases more rapidly than temperature. Once the lower plate is fully emplaced beneath the stationary upper plate, the *P-T-t* paths of the hanging and footwalls of the main thrust diverge: the hanging wall undergoes conductive cooling as it is juxtaposed with the cool sediments atop the downgoing plate, and footwall sediments are conductively heated by the hot lower crust of the stationary plate in near isobaric pressure conditions (Fig. 2-2b).

Recent advances in modelling sediment behavior in subduction zone settings have indicated that the process of relamination could add significant amounts of felsic material to the

lower crust (Gerya and Yuen 2003, Hacker, Kelemen, and Behn 2011, Castro, Vogt, and Gerya 2013, Kelemen and Behn 2016). In the relamination mechanism, sediments transported along the subduction interface undergo partial melting in contact with the asthenospheric portion of the mantle wedge (Castro, Vogt, and Gerya 2013, Gerya and Yuen 2003). The resulting sediment melt forms silicic diapirs that are buoyant with respect to the surrounding mantle wedge. These diapirs rise until they are incorporated, or relaminated, in the lower crust of the overriding plate (Fig. 2-1c) (Hacker, Kelemen, and Behn 2011, Kelemen and Behn 2016).

The *P-T-t* path of the relamination model also begins along a subduction zone type thermal gradient with pressure increasing more quickly than temperature. After the *P-T-t* path crosses the solidus at ultra-high pressures (1-3GPa) and flux melting of sediment along the interface begins, rapid decompression occurs as the relaminant rises through the mantle wedge (Fig. 2-2c) (Hacker, Kelemen, and Behn 2011). The modelling results of Castro, Vogt, and Gerya (2013) produce a diapir of rising, molten, sediment and basalt that is approximately 40 km wide and 20 km thick.

Relamination has not been definitively identified in the field, but the Swakane and Skagit paragneisses of the North Cascades preserve evidence for high peak pressures (up to 1 GPa) and their position in the lower to mid crust indicate that they could be relaminated sediments that were emplaced at ~54-42 Ma (Matzel, Bowring, and Miller 2004, Gordon et al. 2010, Hacker, Kelemen, and Behn 2011). Another locality that is a potential product of relamination is the Bohemian massif of Central Europe (Nahodilová et al. 2014, Schulmann et al. 2014, Kusbach et al. 2015). Bohemian massif felsic granulites preserve evidence of equilibration at ultra-high pressure conditions of 900 degc and 1.7 to 2.1 GPa prior to high temperature metamorphism at 820-840 degc and 1.2-1.4 GPa, determined using phase equilibria modeling in conjunction with ternary-feldspar and Zr-in-rutile thermometry (Liou, Zhang, and Ernst 2007, Nahodilová et al. 2014). The shape of prograde *P-T-t* path of Bohemian massif granulites is broadly similar to the

schematic P-T-t path shown in figure 2-2c, with an initial high-pressure phase followed by decompression after the relaminate rises and subsequent high temperature metamorphism as the diapir is emplaced at the base of the overriding plate. These felsic granulites enclose lenses of garnet and spinel peridotite that have compositions consistent with subcontinental lithospheric mantle in back arc tectonic settings, which are interpreted to represent portions of mantle captured by the felsic diapirs as they rose through the mantle wedge (Kusbach et al. 2015).

This investigation seeks to constrain the prograde *P-T-t* path of the Ivrea-Verbano Zone and compare the result to the characteristic *P-T-t* paths associated with each of the three tectonic models. This will allow for the confirmation or elimination of any tectonic mechanisms as a candidate for the assembly of the IVZ lower crustal section.

Reconstructing prograde *P-T-t* paths from granulite-grade metamorphic rocks is a challenging task, because high pressures and temperatures or overprinting during subsequent metamorphic events can destroy information about the timing and conditions of prograde metamorphism (Redler et al. 2012). The presence of the accessory mineral monazite in IVZ metapelites, however, makes obtaining data from the prograde assembly of the lower crust possible. Monazite , a rare earth element phosphate, is stable from greenschist (~300 ºC) to granulite (~1000ºC) facies conditions, and thus potentially preserves a prograde *P-T-t* record (Lanzirotti and Hanson 1996). Monazite also incorporates concentrations of U and Th in the ppm – wt.% range and has a high U-Th-Pb closure temperature of ~1000ºC. Its ability to retain Pb at high temperatures means that cooling ages are not reset during residence under peak *P-T* conditions (Smith and Giletti 1997). Monazite U-Pb ages in conjunction with major and trace element geochemical data allow us to link time with thermobarometric estimates of *P* and *T* determined from phase equilibria modeling and trace element thermometers to reconstruct the prograde IVZ *P-T-t* path.

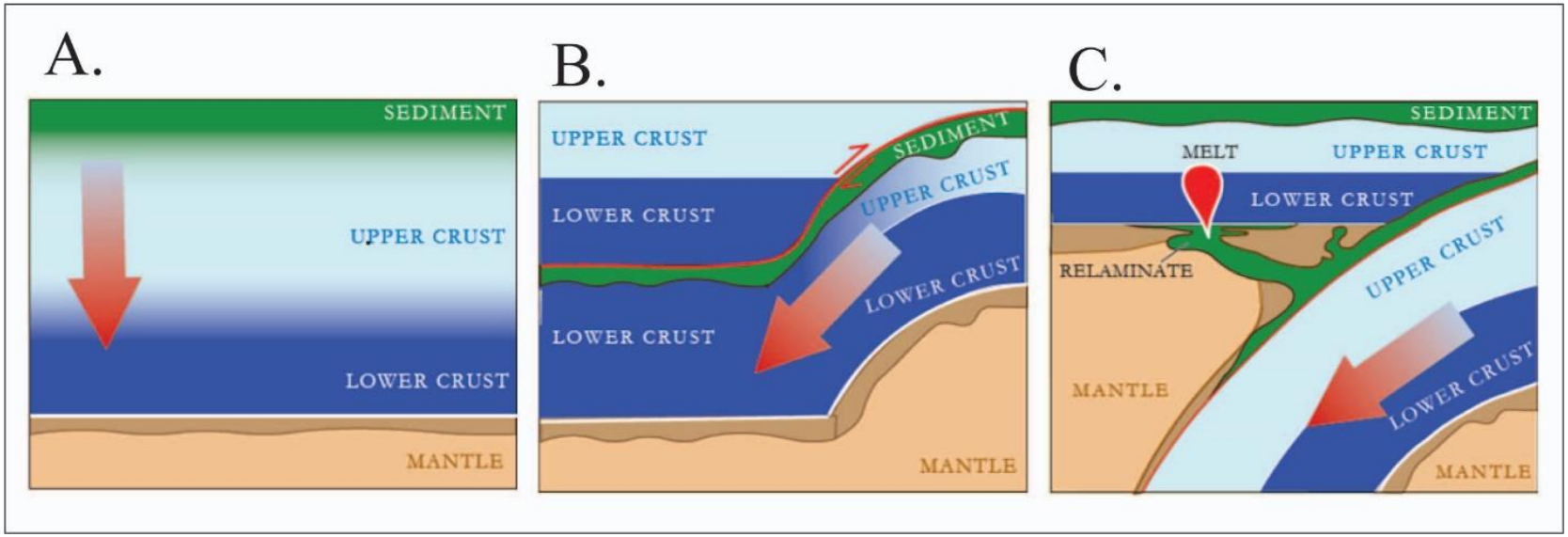

Figure 2-1. Cartoon showing how sediments are transported to lower crustal levels in the A. burial, B. crustal underthrusting, and C. relamination tectonic mechanisms. Red line in B. indicate position of thrust fault separating the two plates, small red arrows show sense of motion across fault. Figure after (Hacker, Kelemen, and Behn 2011)

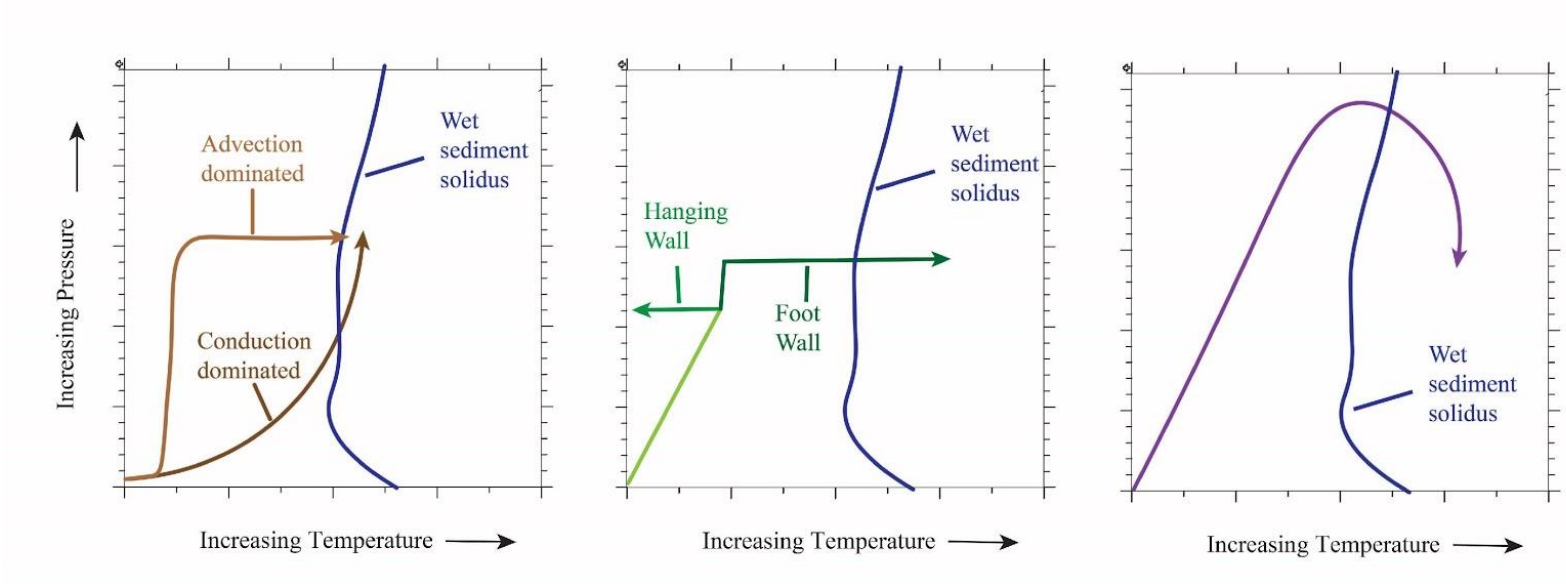

Figure 2-2. Schematic P-T path diagrams for competing tectonic mechanisms. A. Burial, B. Crustal Underthrusting, C. Relamination. Typical wet sediment solidus after (Nichols, Wyllie, and Stern 1994)

Chapter 3

Geologic Background

3.1 Tectonic History

The Ivrea-Verbano Zone (IVZ) in the Southern Alps of northwestern Italy is a section of Hercynian-age middle-to-lower continental crust (Fig. 3-1) (Burke and Fountain 1990, Zingg et al. 1990, Quick, Sinigoi, and Mayer 1995, Sinigoi et al. 1996, Boriani and Villa 1997, Handy et al. 1999). Tilted and faulted into its current position during the Alpine collision, the boundaries of the IVZ are defined to the northwest by the Insubric Line and to the southeast by the Cosseto-Mergozzo-Brissago (CMB) Line (Mehnert 1975, Fountain 1976, Brodie, Rutter, and Evans 1992). The Insubric Line is a 1 km-thick Oligo-Miocene mylonite belt separating the Southern Alpine block, including the IVZ, from greenschist facies rocks that underwent high pressure Alpine metamorphism (Central Alpine block; (Babist et al. 2006) The Permian CMB line is a 6 km-wide transpressional shear zone that divides the IVZ mid to lower crustal section and the Serie dei Laghi mid-upper crustal section (Schmid, Zingg, and Handy 1987, Boriani et al. 1990). Different interpretations exist for the relationship between the IVZ and the Serie dei Laghi; some regard the two sections as a coherent cross section of continental crust (Hunziker and Zingg 1980, Zingg et al. 1990, Henk et al. 1997, Handy et al. 1999, Quick et al. 2003), but Boriani et al. (2016) suggests that the two crustal sections are not related and the Serie dei Laghi was transported into its current position in the early Permian. Metabasites in the IVZ have MORB-type geochemical signatures while Serie dei Laghi metabasites have compositions that are closer to back-arc basalts (Boriani and Giobbi 2004).

3.2 Lithological Units

The IVZ extends ~120 km NNE-SSW following the strike of the Insubric Line and is 14 km across at its widest point. It is dominated by siliciclastic metasedimentary and metaigneous rock, with minor ultramafic rock, quartzite, calcsilicate and carbonate (Fig. 3-1). Each of these rock types are intruded by the voluminous Mafic Complex—a regional (100 km along strike and up to 10 km wide) gabbroic body that was emplaced within the IVZ section following the thermal climax responsible for metamorphism in the metasediments (Barboza, Bergantz, and Brown 1999, Barboza and Bergantz 2000, Quick et al. 2003). Within the IVZ, metamorphic grade increases from amphibolite grade in the southeast to granulite in the northwest; conditions increase perpendicular to both the strike and dominant planar fabric of the IVZ (Fig. 3-1)(Schmid and Wood 1976, Brodie, Rutter, and Evans 1992, Ewing, Hermann, and Rubatto 2013). Even though the IVZ experienced rift-related deformation and heating during the Triassic and Jurassic (Handy et al. 1999) as well as Alpine collision, retrogressive overprinting is minor and restricted to macroscale shear zones (Schmid 1993).

The IVZ siliciclastic sediments have psammitic (SiO_2 between ~53 to 60 wt. %) to pelitic (SiO_2 between ~50 and 77 wt. %) compositions (Redler et al. 2012). These metasediments are often categorized based on their metamorphic grade: Lower structural levels of the IVZ host granulite facies paragneisses called “Stronalites,” while amphibolite facies metasediments found in higher structural levels are referred to as “Kinzigites” (Schmid 1993). Kinzigite unit metasediments are predominately aluminous metapelites, but also include metapsammites and metagreywackes (Redler et al. 2012). Stronalite bulk composition indicates that it has undergone 20–40 weight percent melt loss of a granitic component from Kinzigite precursors (Schnetger 1994, Barboza, Bergantz, and Brown 1999, Barboza and Bergantz 2000). Ultramafic lenses ranging from several kilometer to several meter scale dimensions are dominated by spinel lherzolite and minor cumulus pyroxenite (Sills and Tarney 1984). Ultramafic rocks crop out in

the lowest structural levels of the IVZ near the Insubric Line (Boriani and Giobbi 2004). Geochemical compositions and tectonite fabrics preserved in spinel lherzolites indicate that the lenses originated in the mantle (Voshage et al. 1990). Competing interpretations exist for the origin of these ultramafic bodies, including mafic underplating at the petrological Moho (Vavra et al. 1996) and intercalation during formation of an accretionary prism (Quick, Sinigoi, and Mayer 1995).

The Mafic Complex is a layered igneous intrusion of broadly gabbroic composition that was emplaced between 294 and 286.4 Ma (Henk et al. 1997, Peressini et al. 2007, Guergouz et al. 2018). Exposures of the Mafic Complex occur along the entire length of the IVZ, and its thickness varies from hundreds of meters up to ten kilometers in Val Sesia (Fig. 3-1; Garuti et al, 1980). The base of the intrusion contains peridotites and pyroxenites with cumulate textures, which grade upwards into gabbro-norites, gabbro-diorites and diorites (Brodie, Rutter, and Evans 1992). Slivers of unassimilated metasediments (referred to as septa) incorporated in the Mafic Complex preserve mineral assemblages of antiperthitic plagioclase, garnet, quartz, ± sillimanite, ± rutile, ± graphite, ± corundum; indicative of ultra-high temperature conditions (Sinigoi et al. 1994, Sinigoi et al. 1996).

3.3 Metamorphic History

From amphibolite- to granulite facies conditions, the metamorphic field gradient within IVZ metapelites is defined by decreasing modal abundance of muscovite and increasing modal abundance of alkali feldspar and garnet with increasing intensity of metamorphism (Zingg 1980, Brodie, Rutter, and Evans 1992, Sinigoi et al. 1994, Barboza, Bergantz, and Brown 1999, Rutter et al. 2007). Sillimanite is common throughout the IVZ and is present as fibrous mats associated with biotite in the amphibolite portion of the section, and as crystals with prismatic habit in the granulites (Fig. 3-2) (Schmid and Wood 1976).

In metabasite members of the Kinzigite and Stronalite Formations, increasing metamorphic grade results in the appearance of clinopyroxene and orthopyroxene in hornblende and plagioclase bearing rocks at progressively deeper structural levels (Zingg 1980). Prismatic hornblende changes from green to brown from amphibolite to granulite facies (Sills and Tarney 1984). The changes in the mineralogy of metabasic rocks are partly due to the metamorphic field gradient as well as changes in protolith composition perpendicular to the strike of the IVZ: metabasites near the Insubric Line are depleted in LREE, consistent with a depleted N-MORB type protolith, while metabasites from higher structural levels have enriched LREE patterns that are compatible with an E-MORB type protolith (Mazzucchelli and Siena 1986). Texturally, metabasites transition from nematoblastic to granoblastic with increasing grade (Zingg 1980).

There is a significant body of literature concerning the pressure and temperature evolution of the IVZ (Schmid and Wood 1976, Sills 1984, Kohn and Spear 1990, Zhu and Sverjensky 1992, Henk et al. 1997, Bea and Montero 1999). Initial efforts to quantify metamorphic conditions focused on the application of garnet-biotite Fe–Mg exchange thermobarometry to Kinzigite metapelites, resulting in conditions of 615 ± 30 C at 4.3 ± 1.0 kbar near the CMB line to 810 ± 50°C at 8.3 ± 2.0 kbar near the Insubric Line (Schmid and Wood 1976, Henk et al. 1997). Subsequent investigations have revised IVZ temperature estimates upwards; Luvizotto and Zack (2009) and Ewing *et al.* (2013) applied single-phase solution thermometers (Zr-in-rutile, Ti-in-zircon) to show that peak metamorphic temperatures were between 850 and 1000 °C. Application of phase equilibrium modeling to IVZ metapelites yielded *P-T* conditions from ~3.5–6.5 kbar and 650–730°C in amphibolites from the top of the section to ~10–12 kbar and 900–950°C in granulites from the deepest structural levels (Redler et al 2012). Previous workers have shown that the metamorphic field gradient is steeper than expected in undisturbed continental crust (~0.3 km/kbar; (Burke and Fountain 1990), implying that the section has undergone attenuation following Permian high-temperature metamorphism (Brodie

and Rutter 1987, Brodie, Rutter, and Rex 1989, Henk et al. 1997). A timeline of major metamorphic events in the Ivrea-Verbano Zone is included in figure 3-3.

3.4 Geochronology

Siliciclastic metasediments in the IVZ contain prismatic detrital zircon ≤2.0 Ga interpreted to be derived from calc-alkaline igneous rock (Vavra et al. 1996, Vavra, Schmid, and Gebauer 1999, Peressini et al. 2007, Ewing, Hermann, and Rubatto 2013, Guergouz et al. 2018, Kunz, Regis, and Engi 2018). The youngest zircon cores have U-Pb dates of between ~389 Ma and ~352 Ma (Vavra et al. 1996, Vavra, Schmid, and Gebauer 1999, Kunz, Regis, and Engi 2018), implying that sediment deposition was underway by ~350 Ma at the latest and continued until the onset of regional metamorphism at ~320 Ma (Ewing, Hermann, and Rubatto 2013).

Regional amphibolite-granulite facies metamorphism, responsible for the metamorphic field gradient, initiated at 316 ± 3 Ma (zircon U-Pb dates; Ewing, Hermann, and Rubatto 2013), predating intrusion of the Mafic Complex at ~296 Ma (Pin 1990, Henk et al. 1997, Quick et al. 2003, Peressini et al. 2007) by ~10-30 Ma (Quick, Sinigoi, and Mayer 1994, Barboza, Bergantz, and Brown 1999, Barboza and Bergantz 2000). The regional thermal climax occurred either during or after construction of the IVZ crustal section, and there is no consensus regarding the heat source that caused the regional high-temperature event. Conductive heating associated with intrusion of the Mafic Complex produced a 2 km-wide aureole of upper amphibolite-facies metamorphism with cordierite, hercynite, and andalusite that overprinted the earlier amphibolite- to granulite-facies metamorphism (Zingg et al. 1990, Barboza, Bergantz, and Brown 1999, Snoke et al. 1999, Barboza and Bergantz 2000, Quick, Sinigoi, and Mayer 1994, Schaltegger and Brack 2007). Peak Mafic Complex contact metamorphic temperatures of 900-910°C were reached shortly after it was emplaced at 288 ± 4 Ma, followed by a decrease in temperature of ~100-

200°C by 284 ± 3 Ma and a further ~60-100°C decrease by 259 ± 3 Ma (Peressini et al. 2007, Ewing et al. 2015).

IVZ zircon and monazite also yield late-Permian to early Jurassic U-Pb dates that record post-Mafic Complex tectonic events (Vavra and Schaltegger 1999, Ewing, Hermann, and Rubatto 2013, Ewing et al. 2015). These dates primarily reflect episodes of magmatism and fluid activity that induced recrystallization of pre-existing zircon and monazite (Vavra et al. 1996). Three such events at ~260 Ma, ~240 Ma and ~220-190 Ma are recorded in granulite facies zircon dated by Ewing et al (2013), and amphibolite facies zircon dated by Vavra et al (1999) and are associated with regional scale deep seated magmatism and related metasomatism (Ewing et al. 2015).

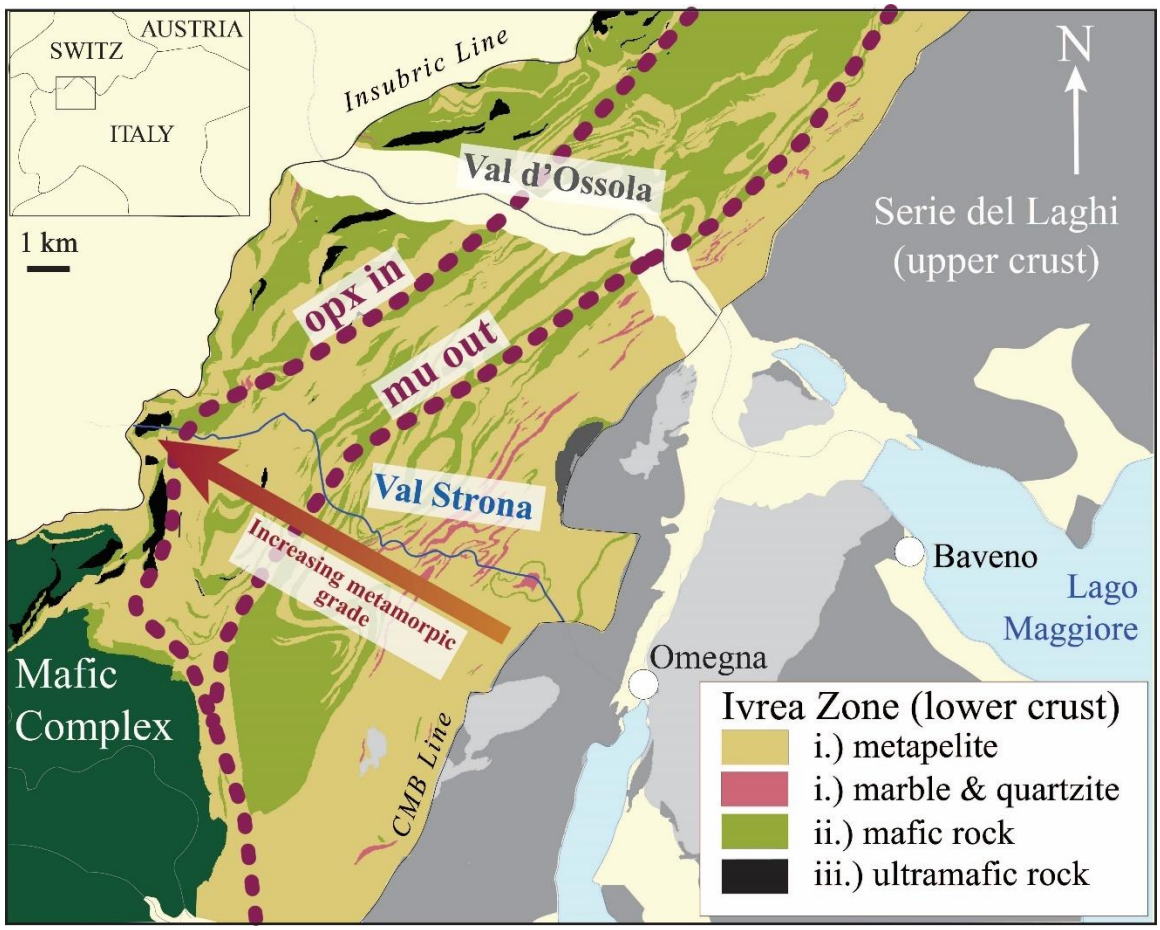

Figure 3-1. Geological map of the Ivrea-Verbano zone (after (Schaltegger and Brack 2007, Redler et al. 2012). Mineral isograds after (Zingg 1980)).

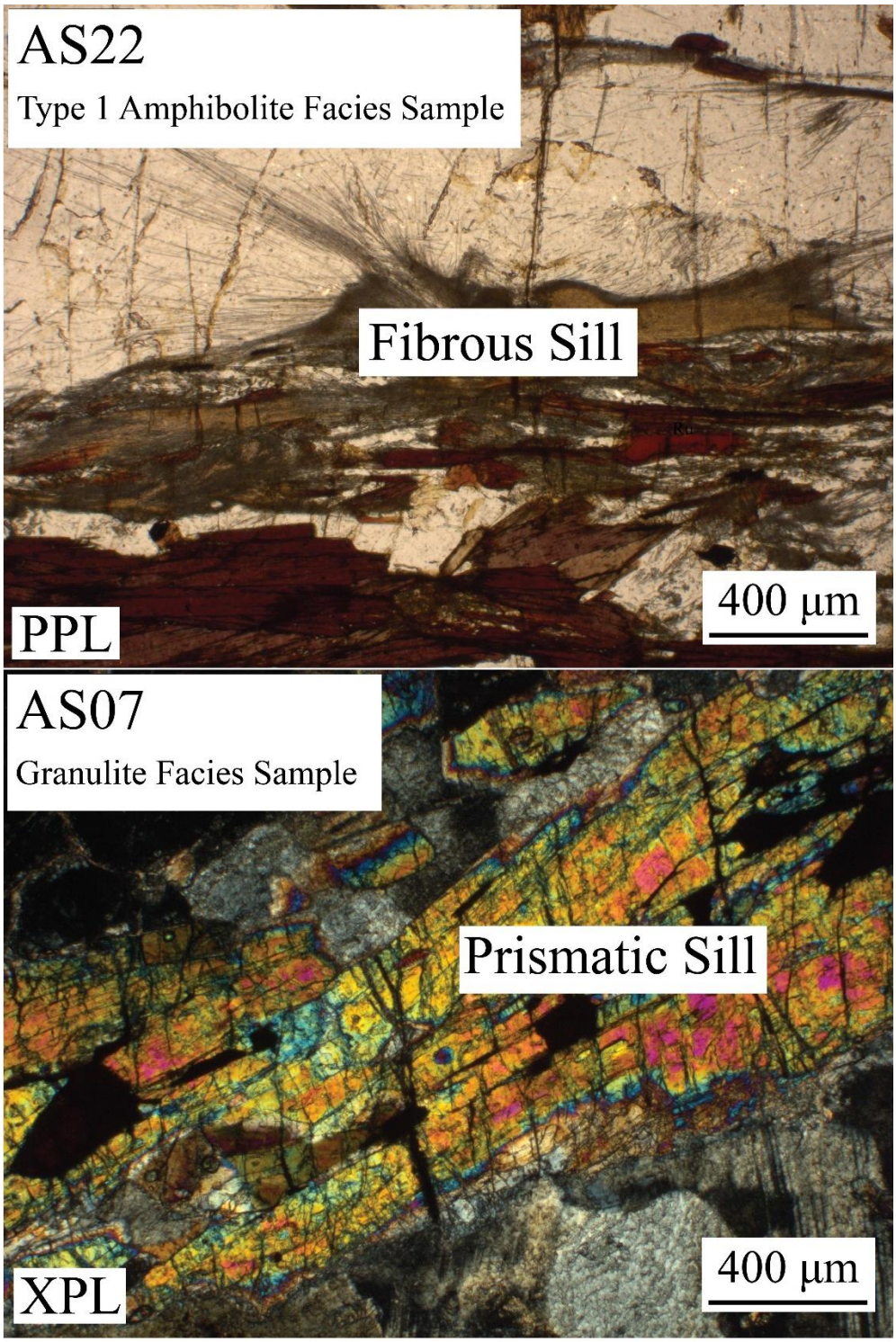

Figure 3-2. Photomicrographs showing difference in habit between fibrous and prismatic sillimanite.

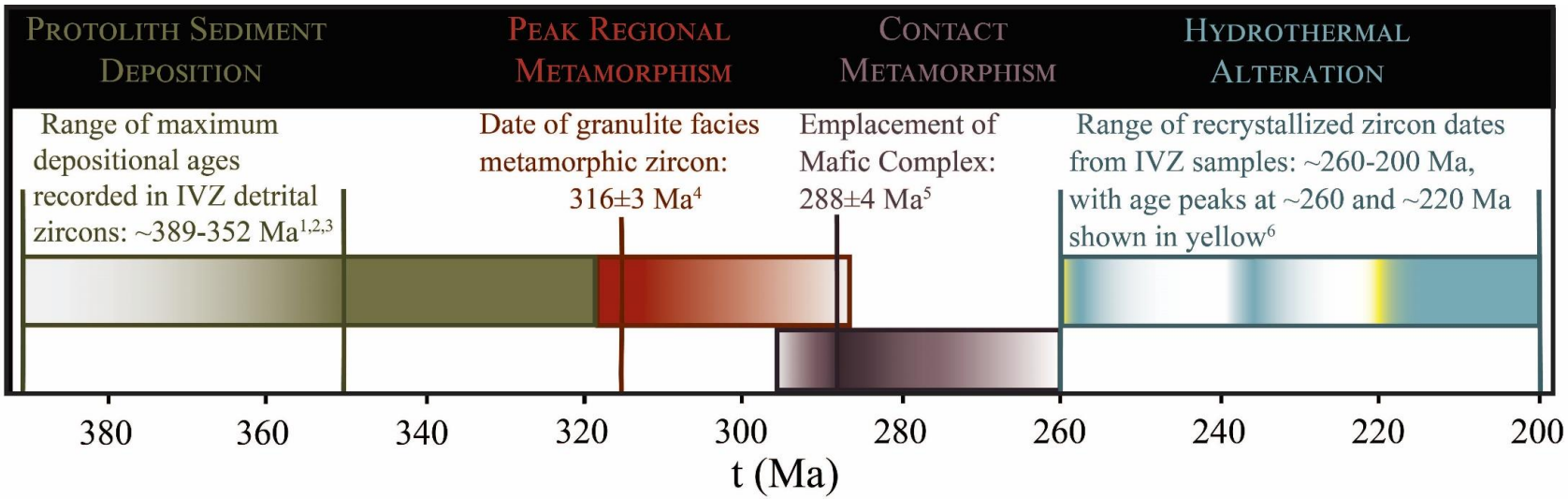

Figure 3-3. Timeline of major metamorphic events in the Ivrea-Verbano Zone (after (Ewing et al. 2015). [1](Kunz, Regis, and Engi 2018),[2](Vavra et al. 1996),[3](Vavra, Schmid, and Gebauer 1999),[4](Ewing, Hermann, and Rubatto 2013),[5](Peressini et al. 2007), [6](Ewing et al. 2015)).

Chapter 4

Sample Petrography

4.1 Sampling Strategy

Eighty samples were collected during field campaigns in 2015 and 2018 from Val Strona di Omegna, a NW-SE trending river valley which exposes rocks from the widest portion of the IVZ section (Fig. 4-1, Brodie et al. 1992). Metapelites containing garnet were collected at ~500 m spacing throughout the valley. Gaps in sampling density along the Val Strona transect, particularly in the lower half of the section, are the result of poor outcrop exposure. Each sample was screened for monazite at the Pennsylvania State University and eleven samples were selected for in-depth petrographical analysis based on structural position and monazite size and abundance (Fig. 4-1; Table 4-1).

4.2 Amphibolites

Amphibolite facies samples fall into two groups: (1) higher grade (MW02, MW03, MW04, AS22) and lower grade (MW19, MW20, MW23, MW25a).

4.2.1 Type 1 Amphibolites:

Type 1 Amphibolites contain Q+ Pl + Kfs + fibrous Sil + Ilm + Grt + Mu + Ru ± Grt with minor Mon, Zr, and Ap (Fig. 4-2b), and are distinguished from type 2 amphibolites by a greater modal abundance of Kfs, Bio, Ru and Grt. Garnet occurs as poikiloblastic crystals between 3 mm and

0.5 mm in diameter, often associated with seams of quartz and plagioclase. Type 1 amphibolites can be differentiated from type 2 amphibolites by (A.) garnet inclusions of primarily quartz with minor oxide phases, rutile and sillimanite (B.) more prevalent fibrolitic sillimanite replacing prograde biotite and (C.) greater crenulation and deformation of mica-defined foliation.

4.2.2 Type 2 Amphibolites: MW19, MW20, MW25, MW23

Type 2 amphibolite metapelites contain Q+ Pl + fibrous Sil + Ilm + Bi + Mu ± Kfs ± Ru ± Grt with minor Mon, Zr, Ap, and rare Xen (Fig. 4-2c). Type 2 amphibolites have a greater modal abundance of idioblastic muscovite, interpreted to reflect prograde growth, compared to Type 1. Where present, garnet is found as hypidioblastic crystals between 0.2 mm and 1 mm in diameter. Of the four type 2 amphibolites investigated, only MW19 was garnet bearing and had fewer garnets that tended to be smaller than type 1 amphibolite sample garnets. Garnet inclusions are primarily quartz and minor oxide phases that are usually clustered in the core of the grain. Fibrous sillimanite after biotite and less commonly muscovite is also found in type 2 amphibolite metapelites. Biotite, muscovite and fibrous sillimanite define a schistosity that is more pronounced than in type 1 samples: outcrops of type 2 amphibolite metapelites tend to be more fissile, and hand samples and thin sections feature prominent 1-2mm wide bands of micas separating pinching and swelling quartzofeldspathic domains.

4.3 Granulites

The sampled granulite facies metapelites from lower structural levels (samples AS06, AS07, AS13) are composed of Q + Kfs+ Ru+ Grt + prismatic Sil + Ilm ± Pl ± Bi ± Mu with minor Mon, Zr, Ap and Ti (Fig. 4-2a). Most garnets are idio- to hypidioblastic grains with pokiloblastic textures ranging in size from 0.4 mm to 5 mm in diameter, but the structurally

deepest sample (AS06) features xenoblastic garnets in 2-3 mm bands that alternate with prismatic sillimanite-rich domains. Inclusions in garnet are primarily quartz and sillimanite, with less common rutile and biotite. Some K-feldspar grains display a myrmekitic texture. Granulite facies metapelite samples have undergone partial melting and have metataxitic structures. Leucosomes (0.5-4 cm wide) are composed of quartz, large (up to 6 mm) K-feldspar, plagioclase, and prismatic sillimanite. Melanosomes (1-2 cm wide) are comprised of garnet, rutile, ilmenite and minor biotite $\pm$ muscovite. The boundaries between the leucosomes and melanosomes become more sharply defined with increasing structural depth.

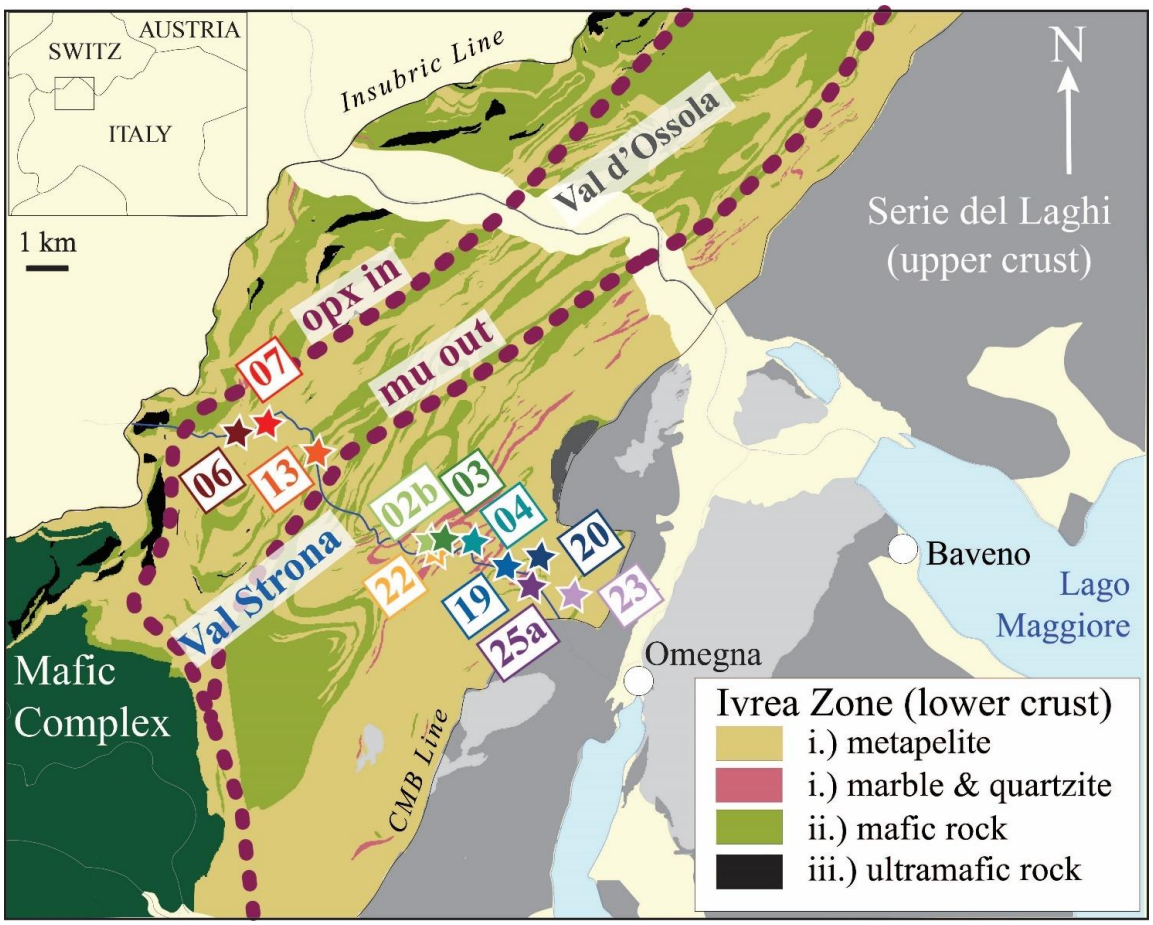

Figure 4-1. Geological map of the Ivrea-Verbano zone showing sample locations (after (Schaltegger and Brack 2007, Redler et al. 2012). Mineral isograds after (Zingg 1980)).

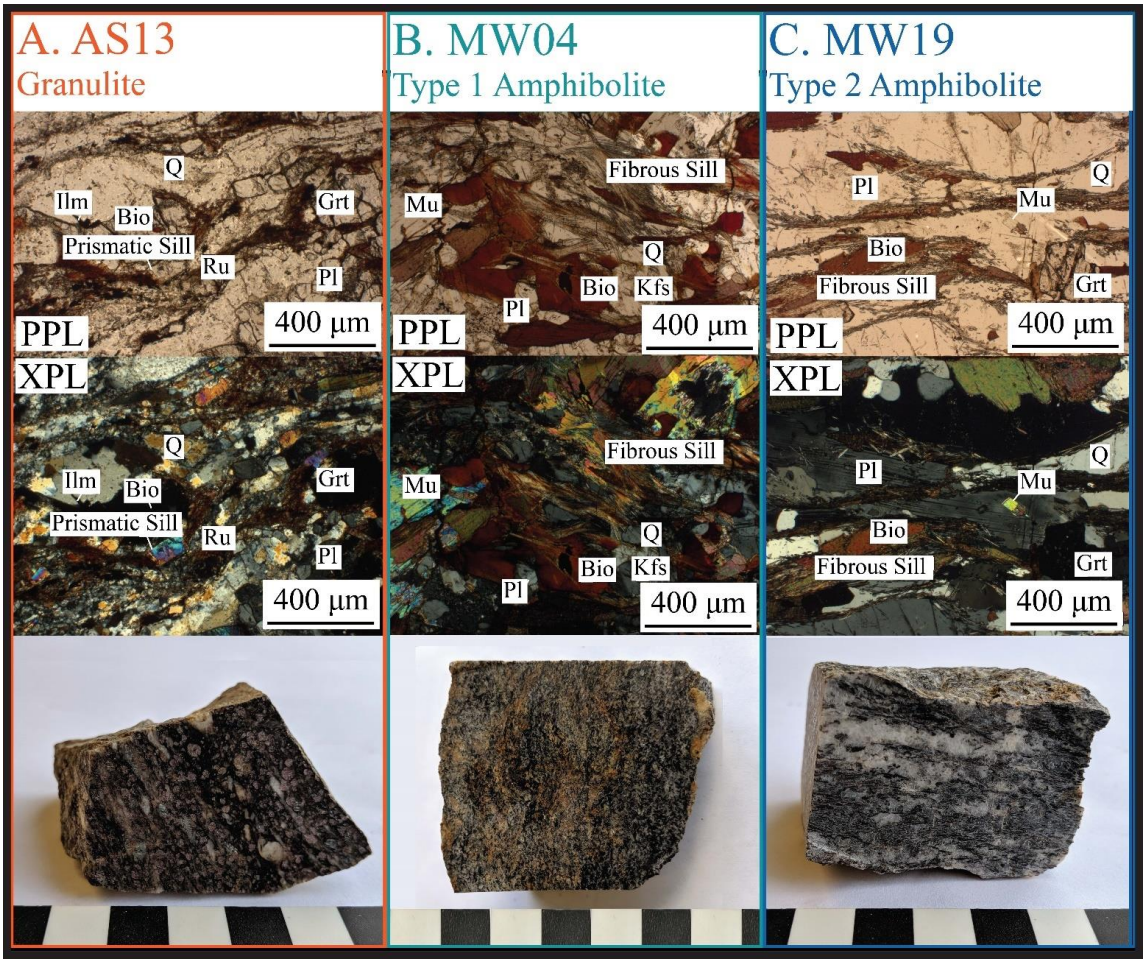

Figure 4-2. Photomicrographs in plane polarized (PPL) and cross polarized (XPL) and hand sample photographs of A. granulite facies, B. type 1 amphibolite and C. type 2 amphibolite representative samples.

Table 4-1. Summary of Petrologic Data:

	Major Phases									Minor Phases					
Sample Name:	Q	Pl	Kfs	Bi	Mu	Ru	Grt	Sill	Ilm	Mon	Zr	Ap	Xen	Ti	Mon size [μm]
AS06	y	n	y	n	n	y	y	pris	y	y	y	y	n	y	50-100
AS07	y	y	y	n	n	y	y	pris	y	y	y	y	n	y	100-200
AS13	y	y	y	y	n	y	y	pris	y	y	y	y	n	y	50-300
MW02	y	y	y	y	y	y	y	fib	y	y	y	n	n	n	50-75
AS22	y	y	y	y	y	y	n	fib	y	y	y	n	n	n	75-200
MW03	y	y	y	y	y	y	y	fib	y	y	y	n	n	n	50-75
MW04	y	y	y	y	n	y	y	fib	y	y	y	n	n	n	30-50
MW19	y	y	y	y	y	n	y	fib	y	y	y	n	n	n	50-300
MW20	y	y	y	y	n	y	n	n	y	y	y	n	y	n	20-100
MW25a	y	y	y	y	n	n	n	n	y	y	y	n	n	n	40-100
MW23	y	y	n	y	y	n	n	fib	y	y	y	n	n	n	50-200

Notes: Q=quartz, Pl=plagioclase, Kfs=K-feldspar, Bi=biotite, Mu=muscovite, Ru=rutile, Grt=garnet, Sill=sillimanite, Ilm=ilmenite, Mon=Monazite, Zr=zircon, Ap=apatite, Xen=xenotime, Ti=titanite. Fib= fibrous habit, Pris=prismatic habit.

Chapter 5

Methods

5.1 Electron microscopy (SEM and EPMA)

All analyses were performed on polished thin sections to link U-Pb dates and trace element concentrations to the monazite textural context within the sample. Monazite grains were identified, located and imaged using energy-dispersive spectroscopy and back scattered electrons on FEI Quanta 200 and FEI Quanta 250 SEMs located in Pennsylvania State University's Materials Characterization Laboratory, using an accelerating voltage of 25 kV. Zoning in Y, Na, Ce, K, La, Sr, Mg, Nd, Ca, Th, Al, Si, U, P, and Fe in monazite was assessed qualitatively with X-ray maps created by Pennsylvania State University's Cameca SXFive electron microprobe (EPMA) using an accelerating voltage of 20 keV, current of ~30 nA, step size of 0.2 μm and dwell time of 25 ms. Quantitative analyses of major element composition of garnet were conducted on the same instrument using an accelerating voltage of 15keV, current of ~30 nA, and on-peak count-times of 10-30 s. Ten elements (Na, Mg, Al, Si, K, Ca, Ti, Cr, Mn and Fe) were measured in traverses (spacing ≥15 μm) for LA ICP-MS data reduction and line scans (spacing 3 μm) to quantify garnet zonation.

5.2 Laser Ablation Split Stream ICP-MS (LASS-ICP-MS)

To link monazite U-Pb date to trace element abundances, individual grains were analyzed at the UC Santa Barbara LASS-ICP-MS facility. A Photon Machines 193 nm excimer laser and HelEx sample cell were used, and data were collected on an Agilent 7700S quadrupole ICPMS.

The analyses were obtained with an 8μm laser spot, using a frequency of 3 Hz, a 25 s ablation time, and a fluence of ~1-2 J/cm^2. The laser first fired two cleaning shots, followed by forty-five analytical shots, with a 20 s delay between analyses. Analyses of IVZ monazite grains were interspersed with analyses of the monazite reference standards 44069 [424.9 Ma, (Aleinikoff et al. 2006)] and Bananeira [509 Ma, Kylander (Kylander-Clark, Hacker, and Cottle 2013, Palin et al. 2013)]; 44069 was the primary standard for U–Pb analyses and Bananeira was the primary standard for trace element analyses. Additional monazite standards FC [55.7 Ma, (Horstwood et al. 2003)], Trebilcock [272 Ma, (Tomascak, Krogstad, and Walker 1996)], and Manangotry [555 Ma, (Horstwood et al. 2003)] were also used as additional monitors of accuracy. This investigation obtained ^{206}Pb-^{238}U ages of 424.3 ± 0.9 Ma for 44069, 512.7 ± 1.3 Ma for Bananeira, 56.76 ± 0.3 Ma for FC-1, 276.0 ± 1 for Trebilcock, and 562.1 ± 3.4 Ma for Manangotry. These ages are accurate to within 0.1, 0.7, 1.3, 1.5, and 1.9% of the reference values, respectively (see appendix A). Data reduction was performed using the Iolite plug-in v. 3.7 (Paton et al. 2011) for the Wavemetrics IgorPro software. IsoPlotR (Ludwig 2003) was used for plotting data on Tera–Wasserburg concordia diagrams (Tera and Wasserburg 1972), and to calculate weighted mean ages. Data were plotted on concordia diagrams with the Stacey-Kramers correction for common Pb (Stacey and Kramers 1975).

5.3 Laser Ablation ICP-MS (LA-ICP-MS)

Trace element compositions of garnets were collected using a Thermo X-Series II Quadrupole ICP-MS with a New Wave UP-213 Laser ablation system at the Pennsylvania State University. The analyses used a 30 μm laser spot, a frequency of 20 Hz, a 40 s ablation time, and a fluence of ~8 J/cm^2. Spot spacing was ≥15μm, and traverses were placed to capture rim-core-rim zoning in garnet. Standardization after every eighth measured spot used primary standard NIST 612 and alternating secondary standards NIST614, BCR and BHVO. Ca values measured

by EPMA provided an internal standard. Data reduction was performed using the Iolite plug-in v. 3.7 (Paton et al. 2011) for the Wavemetrics IgorPro software.

5.4 X-Ray Fluorescence (XRF)

Bulk rock composition for 28 samples was determined using X-Ray Fluorescence (XRF). Analysis of samples from the 2015 suite was completed at the University of Portsmouth using a Rigaku Primus II XRF system. Analysis of 2018 suite samples was performed by Dr. Stanley Mertzman at Franklin and Marshall College using a Malvern PANalytical, Inc. Zetium X-ray fluorescence vacuum spectrometer. Difference in sample weight before and after being heated to 950°C for 1.5 hours was used to determine loss on ignition (LOI). The concentration of ferrous Fe was determined via a modified (Reichen and Fahey 1962) titration method. Uncertainties for major oxides SiO_2, TiO_2, Al_2O_3, MgO, CaO, P_2O_5, and total Fe_2O_3 are <3% and <6% for K_2O, Na_2O and MnO in 2015 suite samples. All uncertainties for 2018 suite analyses are <1%.

5.5 Phase Equilibrium Modelling

5.5.1 THERMOCALC

A pseudosection of granulite sample AS13 was calculated using THERMOCALC in the reduced chemical system, Na_2O–CaO–K_2O–FeO–MgO–Al_2O_3–SiO_2–H_2O–TiO_2–O (NCKFMASHTO), using THERMOCALC version 3.33 (Powell and Holland, 1988; updated October 2009) with dataset ds55 and the following a–X models: biotite, garnet and melt after White, Powell and Holland 2007, cordierite after Holland and Powell 1998, muscovite after Coggon and Holland 2002, plagioclase and alkali feldspar after Holland and Powell 2003, spinel, magnetite, and orthopyroxene after White, Powell and Clarke 2002 and ilmenite, hematite, and low grade magnetite after White et al. 2000.

5.5.2 Theriak Domino

Pseudosections for granulite sample AS13, type 1 amphibolite sample MW04 and type 2 amphibolite sample MW19 were calculated in the chemical system MnO –Na_2O –CaO– K_2O – FeO–MgO– Al_2O_3– SiO_2–H_2O– TiO_2–O (MnNCKFMASHTO) using the Theriak-Domino software package with the Holland and Powell (1998) database (Holland and Powell 1998, de Capitani and Brown 1987). Calculations were performed with dataset ds55 and compatible activity composition models including biotite, garnet and melt after White et al. 2007, cordierite, chloritoid and epidote after Holland and Powell 1998, muscovite after Coggon and Holland 2002, plagioclase and alkali feldspar after Holland and Powell 2003, magnetite and orthopyroxene after White et al. 2002, chlorite after Mahar et al. 1997 and Holland, Baker and Powell 1998, clinopyroxene after Green, Holland and Powell 2007 and ilmenite, hematite, and low grade magnetite after White et al. 2000.

Chapter 6

Results

This study targeted monazite from Kinzigite metapelites to characterize the prograde *P-T-t* path of the Ivrea-Verbano Zone. A total of 66 monazite grains from 11 samples collected from different structural levels throughout the Val Strona di Omegna lower-crustal section were analyzed. Monazites larger than 100 µm were preferentially selected for analysis, but some monazites as small as 30 µm were analyzed. In granulite facies metapelites, monazite range between 75 to 300 µm in diameter, while type 1 and type 2 amphibolite monazite crystals vary between 40-275 µm and 30-275 µm in diameter, respectively.

6.1 U–Pb monazite geochronology

A summary of ^{206}Pb-^{238}U age data for each of the 11 IVZ metapelite samples is provided in Table 6-1. Identifying samples that preserve age data from prior to 300Ma is crucial to reconstructing the P-T conditions associated with the prograde assembly of the IVZ lower crustal section that occurred between approximately 320Ma and 300Ma.

6.1.1 Amphibolite Facies Samples

Type 1 amphibolite samples have ages that range from 262±7.5 Ma to 329±12.8. Sample MW02 yielded only 8 analyses from two monazite, the fewest of any sample. MW02 and MW03 did not feature any spots with ages greater than 300Ma. AS22 has 11 spots older than 300Ma, while MW04 has 3. Preservation of prograde data in type 1 amphibolites is poor, and of only

MW04 has a garnet-bearing mineral assemblage suitable for thermodynamic modelling. Tera–Wasserburg concordia diagrams for type 1 amphibolite samples are included in figure 6-1.

Ages of spots from type 2 amphibolite samples range between 254±3.3 Ma and 331±3.1 Ma. MW19 has 3 spots older than 300Ma while MW25a has only 2. MW20 preserves no data from prior to 300 Ma. While MW23 has 136 spots with dates older than 300Ma, the most of any of the 11 samples analyzed, its mineral assemblage does not feature garnet. Tera–Wasserburg concordia diagrams for type 2 amphibolite samples are presented in figure 6-2.

6.1.2 Granulite Facies Samples

Granulite facies samples have an age range of 194±5.4 Ma to 322±8.5 Ma. AS06 features 5 spots with dates older than 300Ma, while AS07 has 3 spots with dates older than 300Ma. AS13 has the widest spread in dates of any sample, ranging from 194±5.4 Ma, the youngest date in all 11 samples, to 322±8.5 Ma. It has 12 spots with dates older than 300Ma. Every granulite facies sample preserves at least 3 spots with prograde ages and has garnet as a part of its peak mineral assemblage. AS13's wide age range indicates that it grew during 128 million years of the IVZ's metamorphic history. Tera–Wasserburg concordia diagrams for granulite samples are included in figure 6-3.

6.2 Monazite trace element geochemistry

6.2.1 Variations in HREE and Y concentration with age

Rank order plots for type 1 amphibolite sample MW04, type 2 amphibolite sample MW19, and granulite sample AS13. were constructed to characterize the relationship between variations in age and HREE and Y concentration within monazite grains to determine which samples preserve variations in trace element geochemistry associated with the prograde assembly of the IVZ. (Figures 6-4, 6-5, and 6-6). Garnet preferentially takes up Y during growth, so areas of monazite with lower Y concentrations (reflected as cool colored bars on the rank order plots) indicate that garnet was part of the mineral assemblage during monazite growth (Pyle et al. 2001, Spear and Pyle 2010, Hacker, Kylander-Clark, and Holder 2019). A larger Dy/Yb ratio (corresponding to a warmer colored bar on the rank order plot) corresponds to relative depletion of HREE, which indicates that garnet is stable and incorporating HREE at the expense of monazite (Davidson, Turner, and Plank 2012). Type 2 amphibolite samples MW19, MW25a, and MW23 have monazite spots with dates younger than ~295 Ma featuring higher Y concentrations and low Dy/Yb ratios that may be a result of retrograde monazite growth and/or subsequent metamorphic events (Fig. 6-5). Y concentrations and Dy/Yb ratios in type 2 amphibolite facies sample MW20, Type 1 amphibolite samples IVZ18MW22 and MW02, and granulite facies sample AS07 do not vary systematically with age, representing possible decoupling of geochronologic and geochemical during hydrous retrogression due to fluid influx or later metamorphic overprinting (Kelly, Harley, and Möller 2012). Two type 1 amphibolite samples (MW04 and AS22), three type 2 amphibolite samples (MW19, MW20, MW23), and two granulite facies samples (AS06 and AS13) have Y and HREE concentrations that preserve systematic variation with age and feature at least one monazite spot enriched in Y with a higher

Dy/Yb ratio that correspond to a date greater than ~300 Ma. These spots potentially represent changes in the stability of monazite and garnet during the prograde assembly of the IVZ lower crustal section.

6.4 Pseudosection modelling

Phase equilibria modelling was performed on samples MW19, MW04, and AS13. One type 2 amphibolite sample, one type 1 amphibolite and one granulite facies sample were selected to characterize mineral assemblages in different structural levels during prograde and peak metamorphic conditions. The modeled samples feature garnet as part of the peak metamorphic assemblage and have at least one monazite spot with an age greater than ~300 Ma that corresponds to an area relatively enriched in Y with a higher Dy/Yb ratio.

Each sample was modeled under two hydration scenarios- one water saturated intended to represent wet sediments at beginning of prograde path modeled between 300-600 °C, and one with water content based on loss on ignition during XRF analysis (LOI) that represents later stages of metamorphism after initial dehydration. Figures 6-7 and 6-8 shows the *P–T* pseudosections for both bulk compositions for each of the three samples.

The peak P-T conditions as constrained by the mineral assemblage identified in each thin section are indicated the red-filled fields on the water undersaturated sections shaded for increasing variance. Sample MW19 is a type 1 amphibolite facies metapelite with a peak assemblage of Q+Pl+Kfs+Bi+Mu+Grt+Sill+Ilm (Fig. 6-8a). It is difficult to establish petrographically whether sample MW19 underwent partial melting, but the absence of rutile and staurolite coupled with the presence of sillimanite as the aluminosilicate polymorph indicate that it is unlikely that this sample crossed the solidus during peak metamorphism. Sample MW04 is a type 2 amphibolite facies metapelite with a peak assemblage of

Pl+Kfs+Bi+Ru+Grt+Sill+Ilm+Liq (Fig. 6-8b). Muscovite is present in the MW04 thin section, but its low modal abundance (<5%) and raggedy appearance implies that it is likely a retrograde or metastable phase. Fibrous sillimanite in both amphibolite facies samples is often found replacing biotite, indicating that it may be a result of a retrograde reaction. Isolated mats of sillimanite fibers preserved as inclusions in quartz and alkali feldspar, however, provide confirmation that it is part of the peak assemblage under amphibolite facies metamorphism. Sample AS13 is a granulite facies metapelite with a peak assemblage of Pl+Kfs+Bi+Ru+Grt+Sill+Ilm+Liq (Fig. 6-8c). While white mica (muscovite, margarite) is stable from 300-600°C at pressures in excess of 2-9.5 kbar in the water saturated pseudosection, it is not present in the water undersaturated pseudosection at any pressure or temperature (Fig. 6-7c and Fig. 6-8c).

6.5 Yttrium in garnet and monazite thermometry

Yttrium in garnet and monazite (Y-MG) thermometry was performed using the spreadsheet provided by Hacker (2019) to constrain the temperatures of metamorphism attained by samples MW19, MW04, and AS13 during the prograde assembly of the IVZ lower crustal section.

At subsolidus conditions, the Y and HREE concentrations of garnet and monazite are controlled by the compositions of each phase, the bulk composition of the rock, and pressures and temperatures of metamorphism (Spear and Pyle 2010, Hacker, Kylander-Clark, and Holder 2019). The net transfer of P+Y+HREE between coexisting garnet and monazite is described by the following reaction from Pyle *et al.* (2001):

$Y_3Al_2Al_3O_{12}$(YA-garnet) +$Ca_5(PO_4)_3(OH)$(OH-apatite) +$^{25/4}SiO_2$=

$^{5/4}$ $Ca_3Al_2Si_3O_{12}$(Ca-garnet) + $^{5/4}$ $Ca_3Al_2Si_2O_8$(Ca-Plagioclase)

$+ 3YPO_4$ (Y-monazite) $+ {}^{1/2}H_2O$

In metapelites with a low Ca bulk composition like MW19, MW04, and AS13, increasing pressure and/or decreasing temperature causes growth of garnet at the expense of monazite, while decreasing pressure and/or increasing temperature causes growth of monazite and consumption of garnet (Table 6-2)(Spear and Pyle 2010, Hacker, Kylander-Clark, and Holder 2019). All three samples have garnet, apatite, plagioclase, and monazite as part of their peak mineral assemblage, so they are well suited for the application of Y-MG thermometry (Table 4-1).

Garnets from each sample were selected for thermometry based on proximity to monazite grains that preserve prograde ages, with preference for garnets with included or partially included monazite grains. Geochemical data from monazite spots with ages greater than ~298 Ma was paired with all spots from proximal garnets to determine the minimum and maximum temperatures that could have been attained during prograde metamorphism.

Each temperature calculated using the Y-MG thermometer carries an uncertainty of approximately ±30°C based on propagation of uncertainties in pressure, ΔV, ΔH, ΔS, and $\ln(K_{Eq})$ (Pyle et al. 2001). The minimum temperature calculated for MW19 is 440.5±30°C at 319±3.4 Ma and the maximum temperature is 461.1±30°C at 319±3.4 Ma. Temperatures for IVZ 04 vary between 500.8±30°C at 299±2.5 Ma and 542.8±30°C at 300±3.2 Ma. AS13 has a minimum temperature of 472.9±30°C at 313±7.2 Ma and a maximum temperature of 615.2±30°C at 315±8.4 Ma. Monazite spots with ages ranging between 306±9.1 Ma and 322±10.2 Ma all produce temperature estimates in this range.

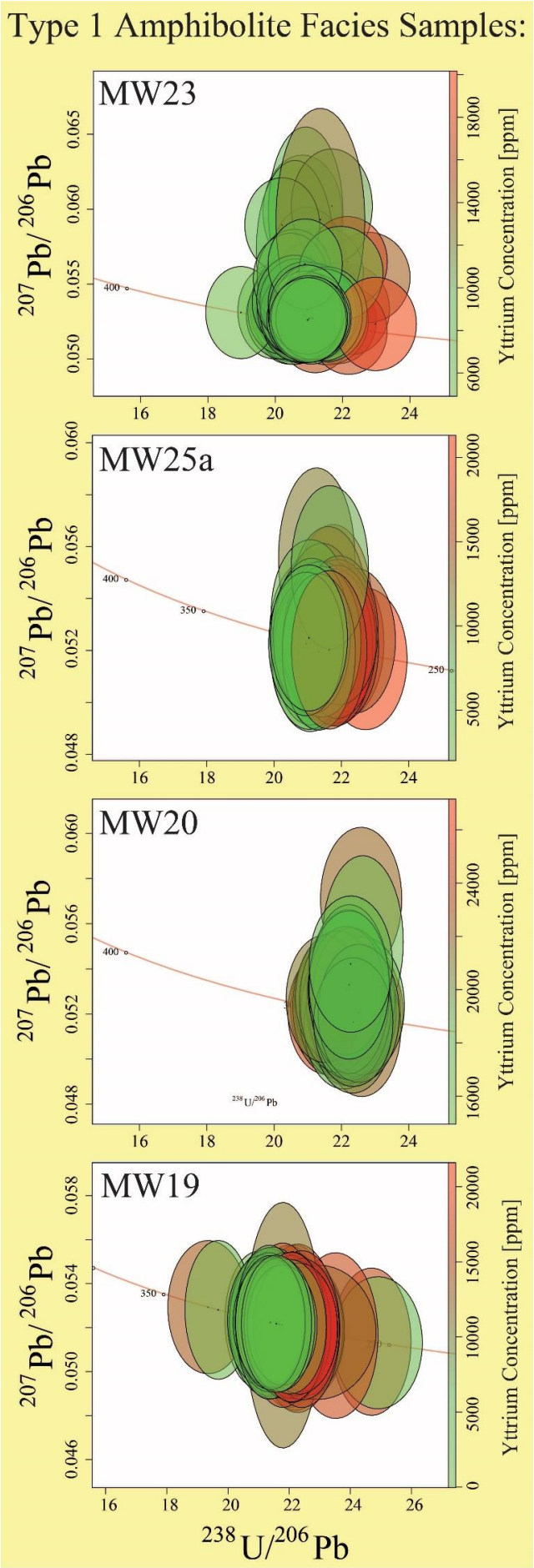

Figure 6-1. Tera–Wasserburg Concordia diagram for type 1 amphibolite samples plotted using IsoPlotR (Ludwig 2003). Size of ovals corresponds to 2σ error associated with uranium and lead LASS ICP-MS measurements. Ovals shaded according to yttrium concentration.

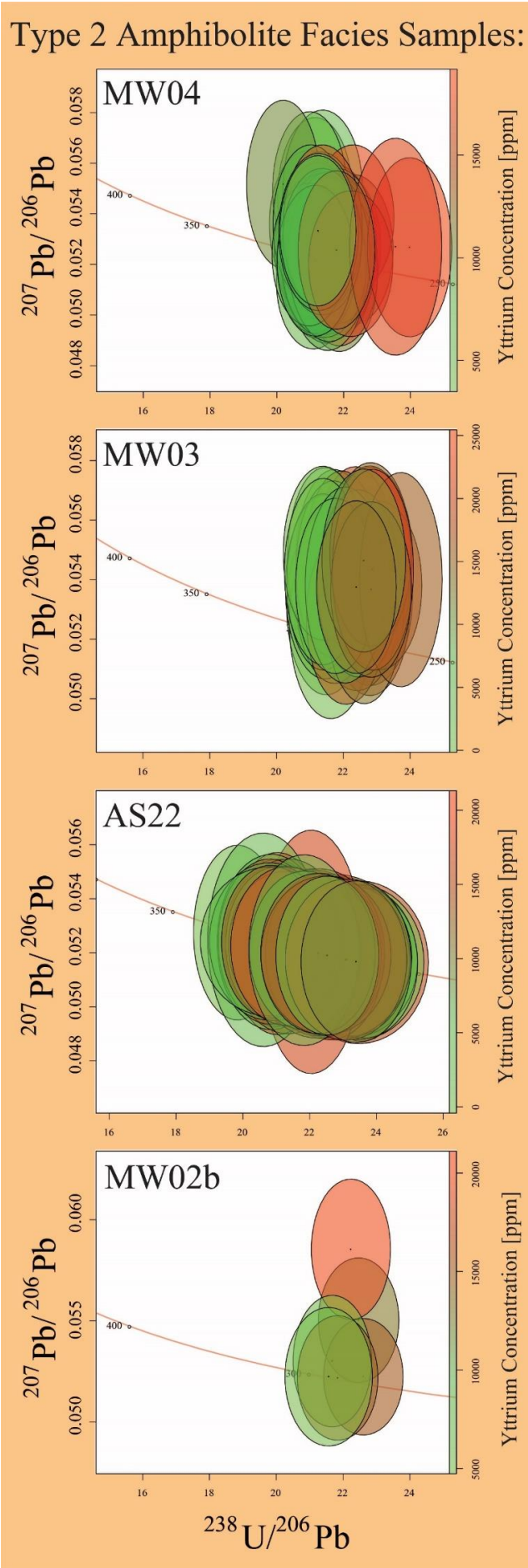

Figure 6-2. Tera–Wasserburg Concordia diagram for type 2 amphibolite facies samples plotted using IsoPlotR (Ludwig 2003). Size of ovals corresponds to 2σ error associated with uranium and lead LASS ICP-MS measurements. Ovals shaded according to yttrium concentration.

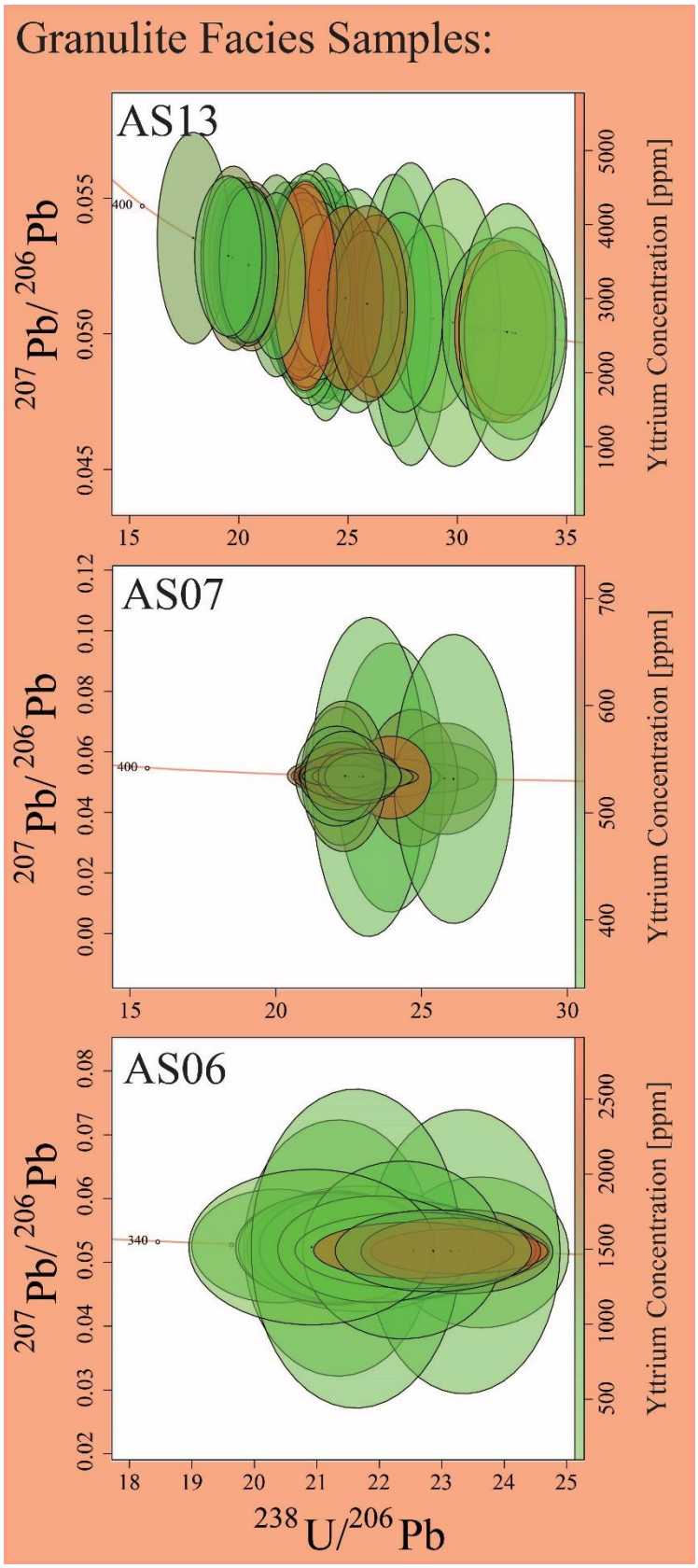

Figure 6-3. Tera–Wasserburg Concordia diagram for granulite facies samples plotted using IsoPlotR (Ludwig 2003). Size of ovals corresponds to 2σ error associated with uranium and lead LASS ICP-MS mea

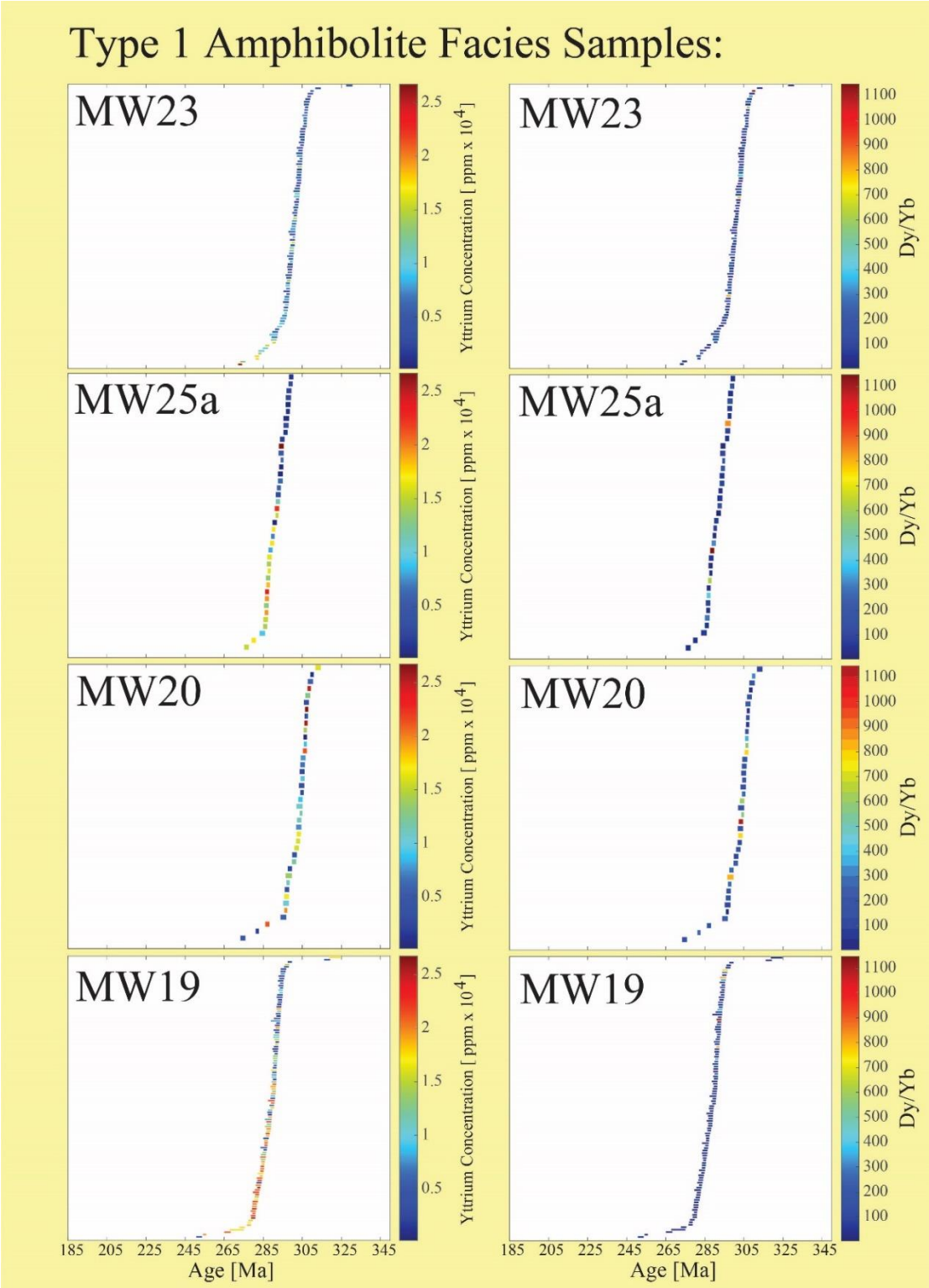

Figure 6-4. Rank order plots showing variation in yttrium concentration on the left and Dy/Yb ratio on the right for type 2 amphibolite samples. Size of bar corresponds to 2σ error associated with U-Pb date.

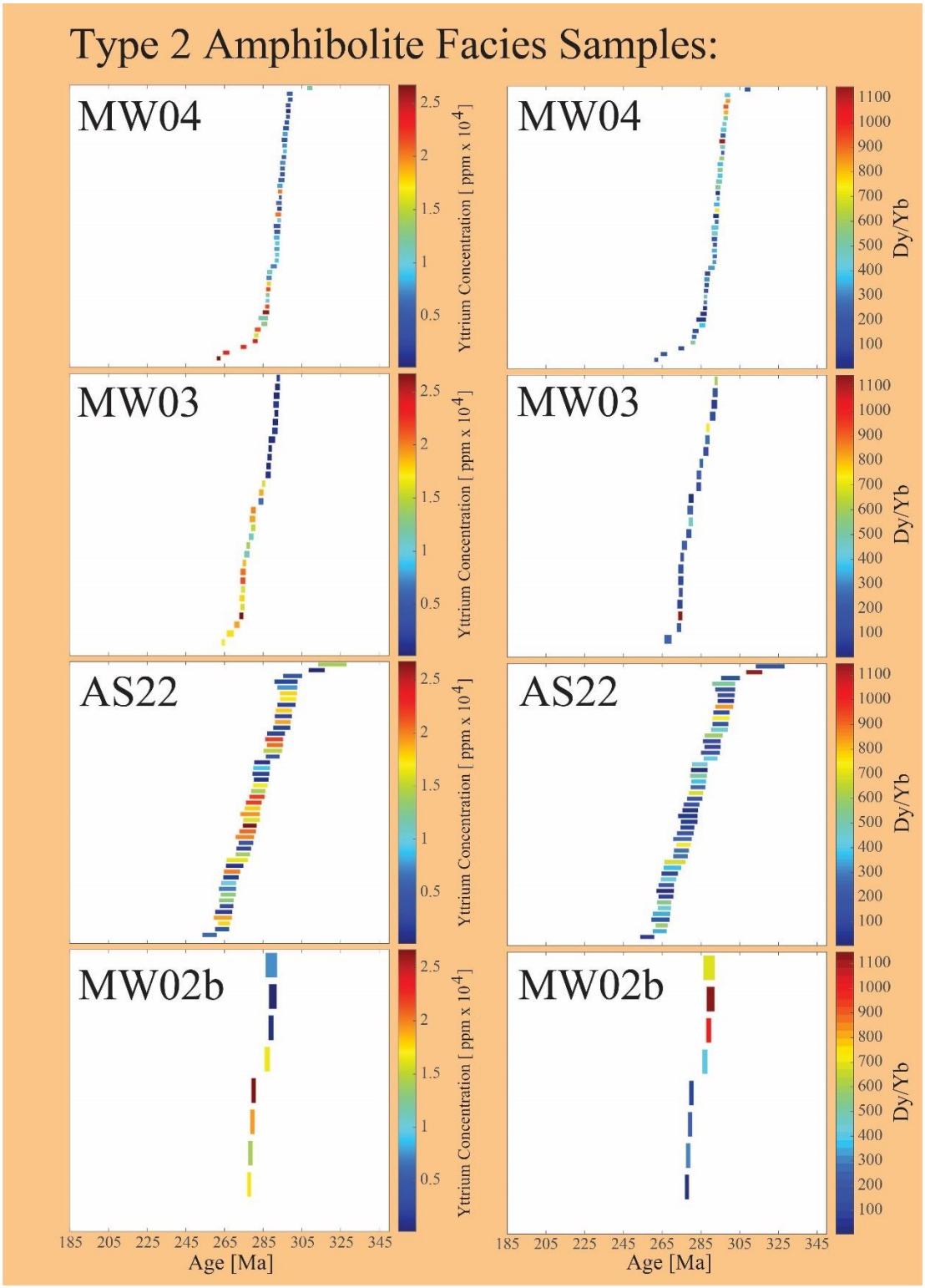

Figure 6-5. Rank order plots showing variation in yttrium concentration on the left and Dy/Yb ratio on the right for type 1 amphibolite samples. Size of bar corresponds to 2σ error associated with U-Pb date.

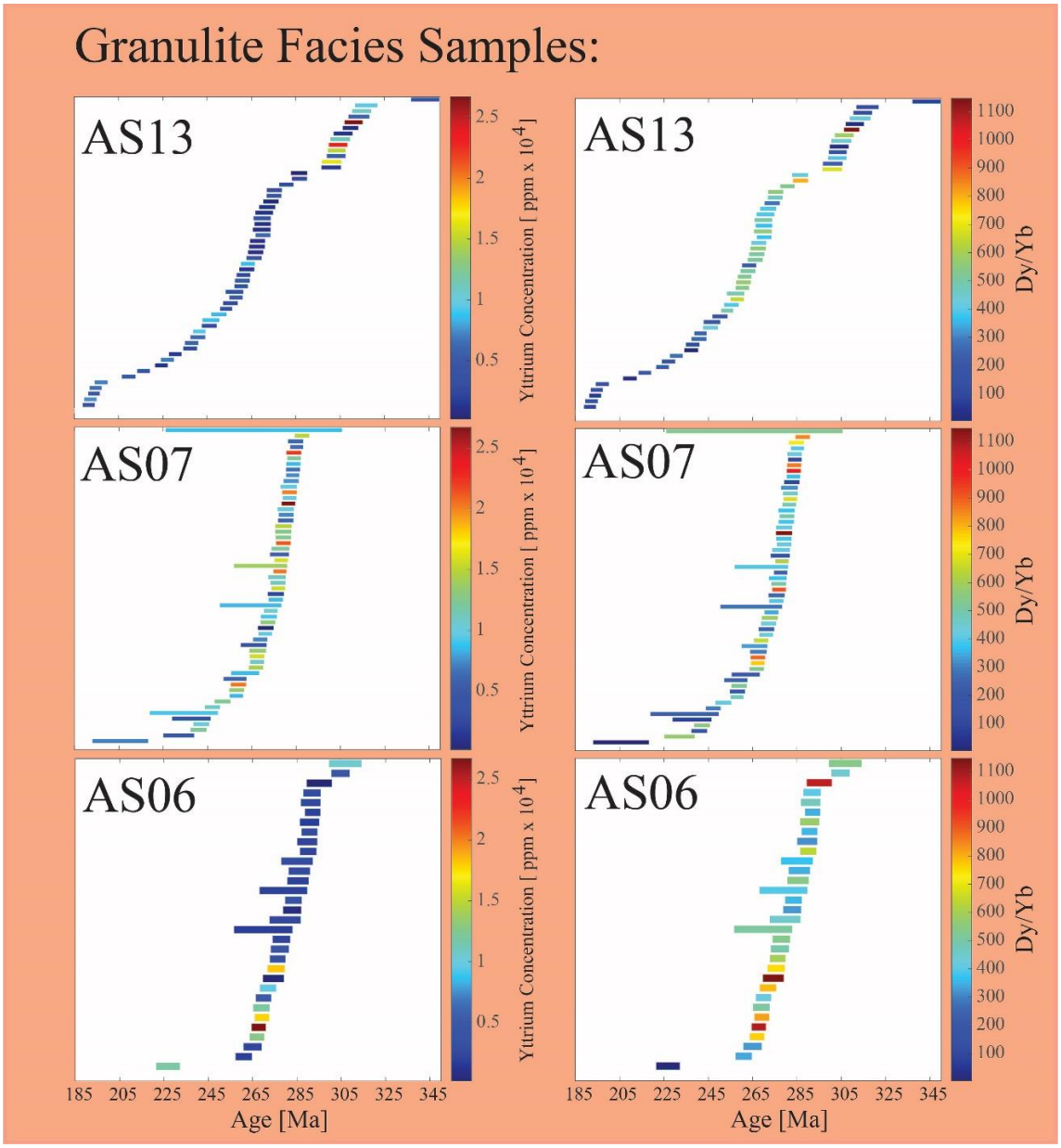

Figure 6-6. Figure 15. Rank order plots showing variation in yttrium concentration on the left and Dy/Yb ratio on the right for granulite facies samples. Size of bar corresponds to 2σ error associated with U-Pb date.

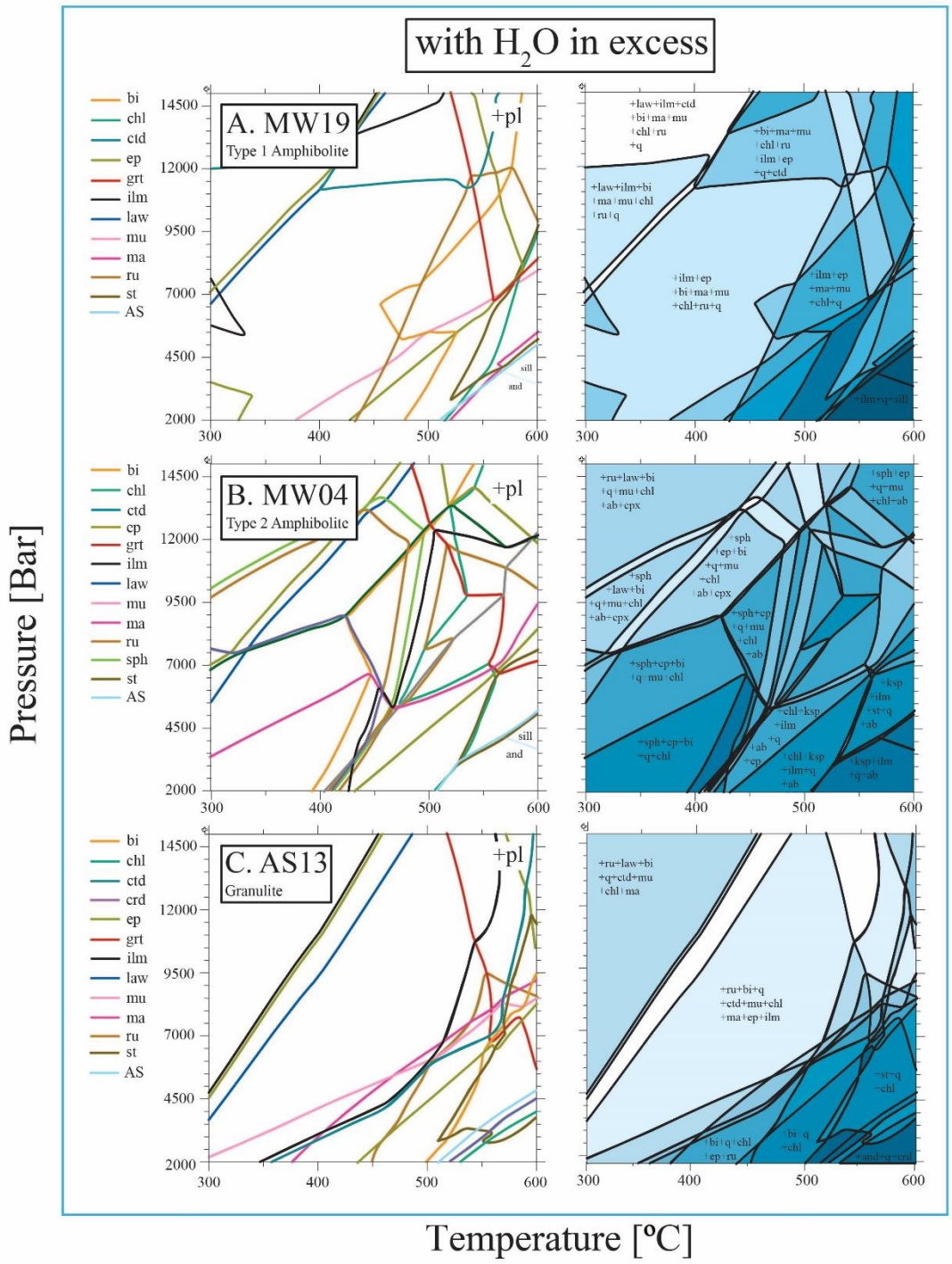

Figure 6-7. Pseudosections calculated using Theriak-Domino version 09.03.2016 de (de Capitani and Brown 1987, de Capitani and Petrakakis 2010)for samples MW19, MW04, and AS13 using a water saturated bulk composition. Colored lines represent reactions producing or eliminating a mineral phase. Darker shading represents larger variance in calculated mineral assemblage.

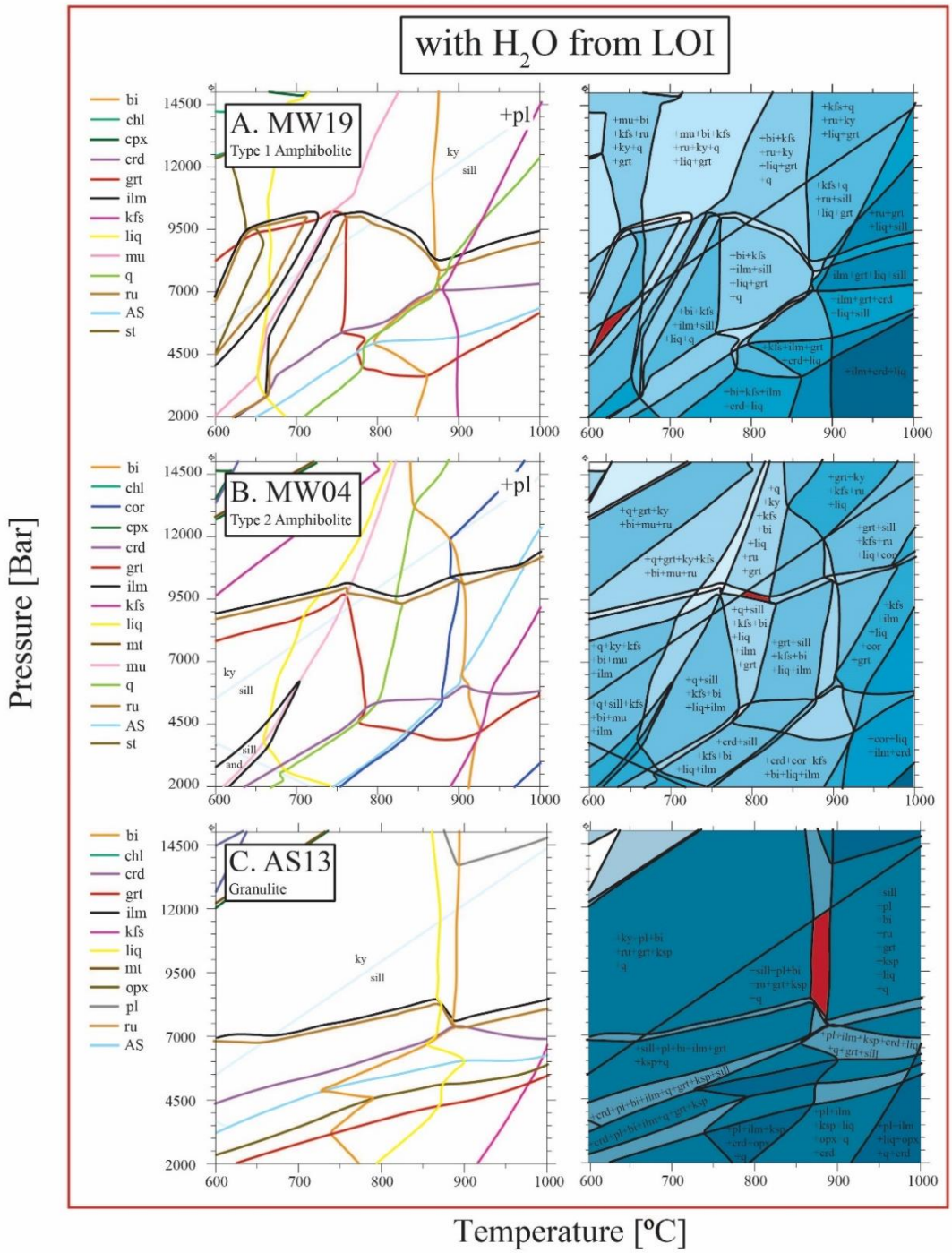

Figure 6-8. Pseudosections calculated using Theriak-Domino version 09.03.2016 de (de Capitani and Brown 1987, de Capitani and Petrakakis 2010)for samples MW19, MW04, and AS13 using a water content derived from the LOI during XRF analysis. Colored lines represent reactions producing or eliminating a mineral phase. Darker shading represents larger variance in calculated mineral assemblage.

Table **6-1**: Summary of monazite U-Pb geochronology results

Sample Name	**Sample Facies**	**Maximum ^{206}Pb-^{238}U age [Ma]**	**Age uncertainty**	**Minimum ^{206}Pb-^{238}U age [Ma]**	**Age uncertainty**
MW23	Type 2 Amphibolite	331	3.1	274	2.3
MW25a	Type 2 Amphibolite	301	2.6	278	2.6
MW20	Type 2 Amphibolite	293	2.6	277	2.5
MW19	Type 2 Amphibolite	325	6.2	254	3.3
MW04	Type 1 Amphibolite	311	3.1	263	2.2
MW03	Type 1 Amphibolite	294	1.9	265	2.0
AS22	Type 1 Amphibolite	329	12.8	262	7.5
MW02	Type 1 Amphibolite	292	6.1	279	2.2
AS13	Granulite	322	8.5	194	5.4
AS07	Granulite	347	14	248	7.5
AS06	Granulite	317	22.5	246	9.3

Table 6-2. Bulk rock composition of samples selected for pseudosection modelling:

Bulk Rock Composition (wt. %)												
Sample	SiO2	TiO2	Al2O3	FeO	MnO	MgO	CaO	Na2O	K2O	P2O5	Total	LOI
IVZ18MW19	56.29	1.27	22.80	9.89	0.19	2.85	0.58	1.28	4.04	0.18	99.37	2.26
IVZ18MW04	53.71	1.18	25.41	8.17	0.11	1.57	2.00	1.95	5.37	0.16	99.63	2.06
IVZ15AS13	57.269	1.405	20.751	11.06	0.119	4.023	1.195	0.707	2.528	0.107	99.8702	0.3372

LOI=Loss on ignition; method of estimating bulk rock H2O contents based on weight loss during XRF analysis

Chapter 7

Discussion

7.1 Characteristics of prograde *P-T-t* paths

Combined, the Y-MG thermometry results and monazite U-Pb dates constrain segments of the prograde *P-T-t* path for type 2 amphibolite sample MW19, type 1 amphibolite sample MW04 and granulite sample AS13.

Monazite from type 2 amphibolite sample MW19 yield temperatures of ~440–461°C at 319 ±6.4 Ma (Fig. 7-1a). Biotite, plagioclase and quartz are present as inclusions, but because quartz and plagioclase are present across all modeled temperatures and pressures and biotite is stable from 2-15 kbar at temperatures <475-575°C, they do not further constrain the prograde *P-T-t* path. However, the absence of rutile in the peak assemblage and as an included phase within monazite constrains maximum pressures to between approximately 2 and 5 kbar. The prograde *P-T-t* path terminated at 600-650 °C and 4.5-6.5 kbar as constrained by the peak mineral assemblage (Q+Pl+Kfs+Bi+Mu+Grt+Sill+Ilm) observed in MW19 (Fig. 7-2a).

The prograde *P-T-t* path of type 1 amphibolite MW04 passed through ~498-543 °C between ~298 and 300 Ma (Fig. 7-1b). While ilmenite is included in 5 of the 8 analyzed monazite grains, no grains preserve rutile inclusions, which indicates that pressures could not have exceeded 11.5 kbar during this segment of the *P-T-t* path. Several other MW04 monazite grains exhibit biotite inclusions, but U-Pb dates from these grains range from ~295-265 Ma; thus, biotite stability is not a useful constraint on pressure during the prograde assembly of the IVZ lower crustal section. The results of pseudosection modelling do not indicate a minimum pressure for MW04's *P-T-t* path. MW04's peak mineral assemblage

(Pl+Kfs+Bi+Ru+Grt+Sill+Ilm+Liq) determines that its prograde path ended at 775-850°C and 9-9.5 kbar (Fig. 7-2b).

For granulite sample AS13, the *P-T-t* path crossed between ~473-615 °C, at ~306-322 Ma; the presence of rutile and ilmenite as inclusions in monazite older than 300 Ma indicates that pressures must have been in excess of 3-8 kbar during this period (Fig. 7-1c). The peak assemblage (Pl+Kfs+Bi+Mu+Ru+Grt+Sill+Ilm+Liq) indicates that AS13 reached 860-870°C and 7-11 kbar at the terminus of its prograde path (Fig. 7-2c).

A range of possible thermal gradients during the prograde *P-T-t* path of the IVZ lower continental crust can be calculated using the results of the Y-MG thermometery and minimum and maximum pressure constraints from pseudosection modelling. Prograde thermal gradients calculated for samples MW19, MW04, and AS13 are 3.4-7.9°C/km, 1.3-12.2°C/km, and 2.5-8.1°C/km, respectively.

7.2 Testing models for sediment incorporation into the lower crust

7.2.1 Comparison of expected thermal gradients

The *P-T-t* constraints presented in chapter 2 permit evaluation of three tectonic mechanisms for assembly of metasedimentary continental lower crust. Burial incorporates sediments from the Earth's surface at lower crustal depths via the addition of crustal material by overplating of volcanic and plutonic rocks, or by prolonged sedimentation. If burial occurs at rates faster than the rate of heat conduction—reflected by a Peclet number ($Pe = \frac{Rate\ of\ Heat\ Transport\ by\ Convection}{Rate\ of\ Heat\ Transport\ by\ Advection}$) greater than 1—sediments will follow a near-isothermal prograde *P-T-t* path. If burial is slow, however, temperatures of metamorphism

will increase according to inputs from mantle heat flow and radiogenic heating, resulting in a prograde *P-T-t* path defined by a continental geotherm. In the IVZ, available detrital zircon U-Pb dates indicate the maximum age of sediment deposition is ~350 Ma (Kunz, Regis, and Engi 2018). If ~350 Ma corresponds to the time at which each of the samples was deposited at the Earth's surface (0 kbar), burial rates range from 0.24-0.51 km/Ma for sample MW19, 0.15-0.82 km/Ma for sample MW04 and 0.50-1.26 km/Ma for sample AS13. Peclet numbers for IVZ metapelites were calculated using the equation $Pe = \frac{v*L}{\kappa}$, where v is burial rate, L is burial depth as indicated by pressure constraints and κ is a thermal diffusivity of ~$1x10^{-6}$ m^2/s. Given that the range of Peclet numbers shown on Figure 7-3 all feature Pe values <1, it is reasonable to assume that burial to lower crustal depths would have occurred under a conduction-dominated thermal regime. If burial were responsible for the construction of the IVZ lower crustal section, the shape of the prograde P-T-*t* path for each sample should reflect pressures that increase along a lithostatic gradient and temperatures that increase along a continental geothermal gradient defined by radiogenic heating and conductive heat loss. Typical values for a continental geothermal gradient are estimated to be approximately 25°C/km at shallow crustal levels and decrease to ~16°C/km at 40 km depth (DiPietro 2013). Given the thermal gradients calculated for samples MW19, MW04, and AS13 are too low to be consistent with a continental geotherm at 3.4-7.9°C/km, 1.3-12.2°C/km, and 2.5-8.1°C/km, respectively, this mechanism is an unlikely candidate for the construction of the IVZ lower crustal section.

Metasediments emplaced into the lower crust by crustal underthrusting or relamination are expected to follow a prograde path characterized by thermal gradients and rates akin to modern-day subduction zones of approximately 5-10 °C/km (Penniston-Dorland, Kohn, and Manning 2015, Syracuse, van Keken, and Abers 2010). Relamination is modeled in subduction zone settings where the downgoing plate dips at angles ranging between 10-70°, and the

downgoing plate in crustal underthrusting settings dips at about 20-60° (Allis 1981, Syracuse, van Keken, and Abers 2010, Xu et al. 2015), so increases in pressure and temperature with depth in the initial phases of the prograde path are broadly similar for both mechanisms.

The calculated thermal gradients for the IVZ samples are consistent with a modern-day - subduction zone setting, with the exception of sample MW04 where temperatures obtained from trace element thermometry correspond to a younger age (300 Ma) than the temperatures associated with AS13 and MW04 (305-322Ma), so the elevated thermal gradient could be the result of the initial stages of the intrusion of the Mafic Complex, which reached its maximum thermal input at ~296 Ma (Barboza, Bergantz, and Brown 1999). Alternatively, the higher thermal gradient inferred for sample MW04 could also reflect a longer period of equilibration (~20 Myr) at lower crustal levels after being emplaced at ~320-315 Ma.

It is acknowledged that these values assume a linear gradient between the calculated depth of the sample and the Earth's surface and do not account for curvature in the thermal gradient introduced by advection and heat production. Regardless, these calculations provide a new constraint on the prograde metamorphic history of these high-grade rocks.

7.2.2 Comparison of expected petrographic observations

While the combined results of Y-MG thermometery and radiometric dating of IVZ monazite do not fully constrain the prograde *P-T-t* path, petrographic evidence collected from thin section analysis allows for further assessment of the competing tectonic mechanisms.

In the relamination hypothesis, as presented in Hacker, Kelemen and Behn, 2011, sediments are subducted to depths greater than 50 km along the slab interface, where they may attain ultra-high pressure (UHP) conditions of ~800-1050°C and ~30 kbar and melt. The felsic relaminate portion of the melt is positively buoyant with respect to the mantle wedge. The

relaminate rises diapirically and is emplaced at lower crustal levels under pressures and temperatures of approximately 700°C and 10 kbar. Accordingly, the presence of UHP mineral phases in lower crustal sediments would provide strong support for the relamination hypothesis. The IVZ metapelites investigated in this study do not preserve any evidence of equilibration at ultra-high, or high-pressures; UHP minerals like coesite or diamond are absent as included phases, as well as other high-grade minerals like sanidine that might been stable at peak relamination conditions.

Previous workers (Schmid, Zingg, and Handy 1987, Zingg 1980) have observed rare kyanite grains with sillimanite overgrowths as part of the mineral assemblage of Kinzigite metasediments, however, no kyanite or kyanite overgrowths were found in any of the 80 samples studied in this investigation. The absence of kyanite in the IVZ15AS and IVZ18MW sample suites further suggests that peak pressures were less than ~9.5-15 kbar and not high enough to be consistent with the relamination hypothesis. While the presence of UHP mineral phases would have been a strong indication that the IVZ metapelites were incorporated into the lower crust through relamination, the absence of these phases does not dismiss relamination as a viable hypothesis, as it is possible for relaminated sediments to undergo a complete mineralogical re-equilibration at the base of the crust and not preserve metastable UHP phases (Hacker, Kelemen, and Behn 2011)

7.2.3 Comparison of expected field observations

Observations of outcrop scale features and the relationships between different IVZ lithologies can also help distinguish between the competing tectonic mechanisms. No clear primary sedimentary structures like crossbedding are preserved in IVZ metapelites, quartzites or calc-silicate rocks. Original bedding relationships between metasedimentary layers are nearly

impossible to discern from jointing and other tabular field relationships between subunits (Fig. 7-4). Destruction of sedimentary features is expected in the relamination mechanism during melting and viscous flow and could also result from deformation during crustal underthrusting. In the burial hypothesis, however, at least some local scale preservation of these features is likely. Later periods of deformation and metamorphism could have obliterated some sedimentary structures in IVZ metapelites, but their widespread absence throughout the section is further evidence that the burial hypothesis is not a viable mechanism for assembly of the lower crust. Further, the tabular nature of outcrop scale structures in the IVZ are not consistent with the relamination hypothesis: melted sediments that rose through the mantle wedge as diapirs would be expected to undergo chaotic mixing on their ascent and not retain any of their previous structure.

7.3 Future Work

More work is needed to fully constrain the prograde path of IVZ metasediments. The primary obstacle is the scarce preservation of geochronological and geochemical data from prior to ~300 Ma. IVZ monazite do retain information from this period, but to provide additional constraints it is necessary to investigate other minerals that grew during the prograde assembly of the IVZ lower crustal section. Determining the age of garnet growth via Lu-Hf geochronometry is key to characterizing earlier portions of the IVZ *P-T-t* path: garnet age data would further refine the timing of the temperatures calculated using the Y-MG thermometer, and could also be used to improve prograde pressure estimates by linking included phases to the results of pseudosection modelling. In samples from higher structural levels, monazite is prevalent and occasionally preserves ages greater than ~300 Ma but lacks garnet as part of the peak assemblage. These samples do feature prograde biotite and white mica, so the use of the Ti-in-biotite thermometer of Henry and Guidotti, 2002 in conjunction with the Si-in-phengite barometer of

Massonne and Schreyer, 1987 could have promise in constraining the *P-T-t* path in additional samples.

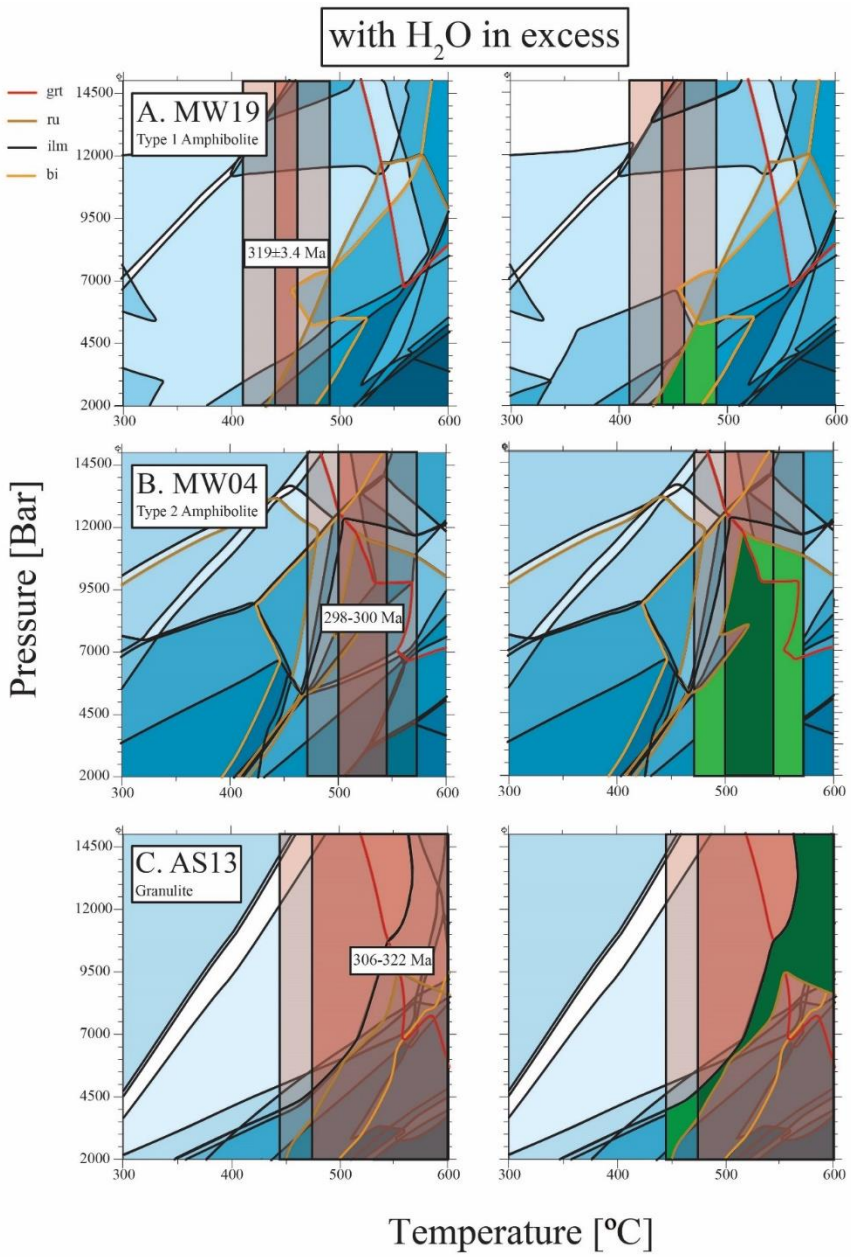

Figure 7-1. Pseudosections calculated using Theriak-Domino version 09.03.2016 de (de Capitani and Brown 1987, de Capitani and Petrakakis 2010)for samples MW19, MW04, and AS13 using a water saturated bulk composition. Darker red shaded boxes represent calculated temperature interval for indicated age period, lighter red shaded box represents error associated with calculated temperatures. Colored lines represent reactions producing or eliminating a mineral phase that constrains pressure. Darker shading represents larger variance in calculated mineral assemblage. Green areas show pressure constrained area the prograde P-T-t path passes through.

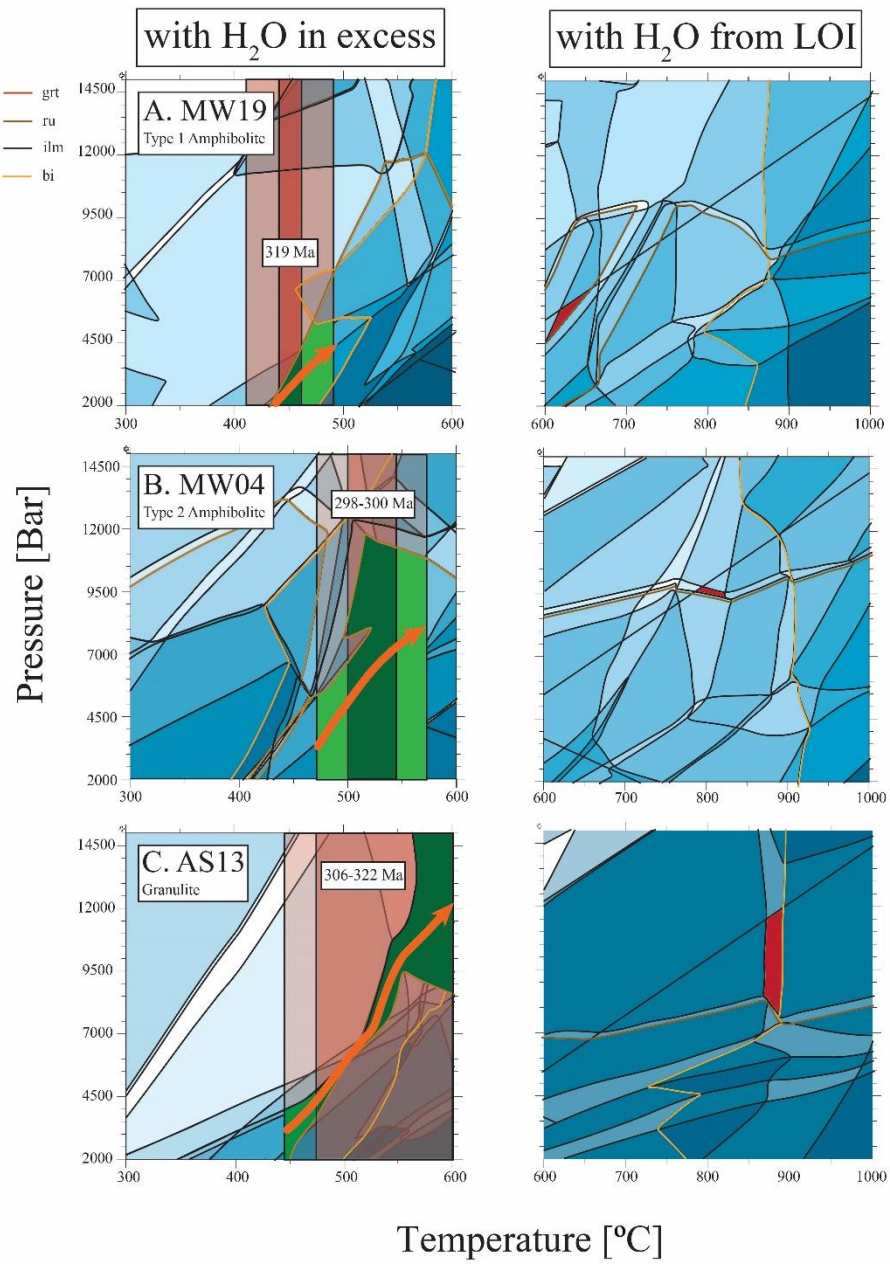

Figure 7-2. Pseudosections calculated using Theriak-Domino version 09.03.2016 de (de Capitani and Brown 1987, de Capitani and Petrakakis 2010)for samples MW19, MW04, and AS13 using a water saturated bulk composition on the left and a water content derived from the LOI during XRF analysis on the right. In the left column, darker red shaded boxes represent calculated temperature interval for indicated age period, lighter red shaded box represents error associated with calculated temperatures. Colored lines represent reactions producing or eliminating a mineral phase that constrains pressure. Darker shading represents larger variance in calculated mineral assemblage. Green areas show pressure constrained area the prograde P-T-t path passes through. Orange arrow represents possible P-T path. In the right column, red filled area indicates peak metamorphic conditions where prograde P-T path ends.

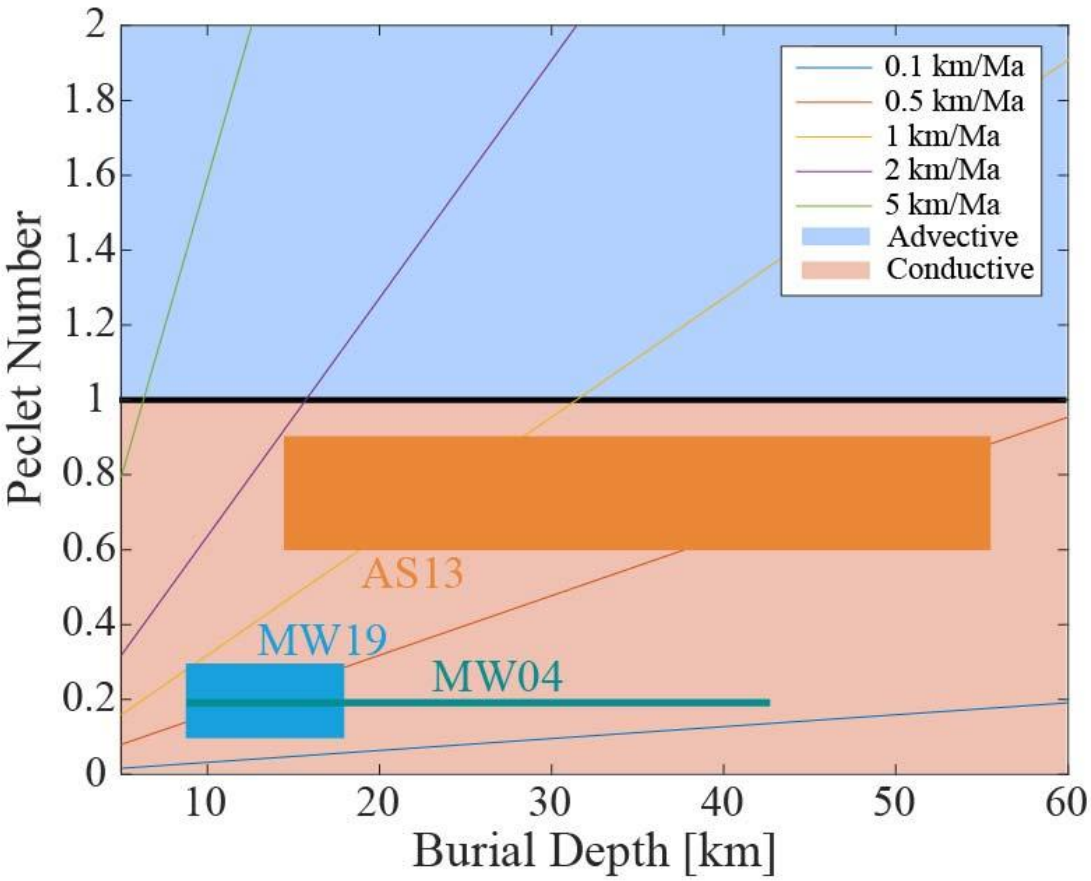

Figure 7-3. Plot showing variation in Peclet number with depth for a variety of burial rates. Blue shaded area where Peclet number is greater than one indicates heat transport is dominated by advection, while red shaded area where Peclet number is less than one indicates heat transport is dominated by conduction. Typical sedimentation rates shown as colored lines, with values indicated in legend. Colored boxes represent range of possible Peclet numbers for type 1 amphibolite MW19 (blue), type 2 amphibolite MW04 (teal) and granulite AS13 (orange) based on possible burial rates and maximum burial depths indicated by psuedosection modeling. All burial depth and rate estimates for IVZ metapelites would undergo heat transport by conduction.

Figure 7-4. Photograph showing sample location for MW04. Jointing and tabular structures are visible, but no protolith bedding can be identified. Dr. Andrew Smye for scale.

Chapter 8

Conclusions

The Y-MG thermometry results, monazite U-Pb dates, and pseudosection modelling presented in this investigation serve to characterize segments of the prograde *P-T-t* path and identify peak metamorphic conditions for three metapelites from the IVZ lower crustal section. Type 2 amphibolite sample MW19 experienced pressures and temperatures of 2-5 kbar and~440–461°C at 319 ±6.4 Ma before equilibrating at 600-650 °C and 4.5-6.5 kbar. The prograde *P-T-t* path of type 1 amphibolite MW04 passed through ~498-543 °C between ~298 and 300 Ma at pressures below 11.5 kbar and experienced peak metamorphic conditions of 775-850°C and 9-9.5 kbar. For granulite sample AS13, the *P-T-t* path crossed between ~473-615 °C and 3-8 kbar at ~306-322 Ma before reaching 860-870°C and 7-11 kbar at the terminus of its prograde path. Crustal underthrusting is the preferred mechanism for construction of the IVZ lower crustal section. Thermal gradients for type 1 amphibolite MW19, type 2 amphibolite MW04 and granulite AS13 are 3.4-7.9°C/km, 1.3-12.2°C/km, and 2.5-8.1°C/km, respectively The similarity of these values to modern-day subduction zone thermal gradients of 5-10 °C/km supports both the crustal underthrusting and relamination mechanisms. While the lack of preservation of UHP phases and chaotic structures cannot conclusively rule out relamination, the ultramafic lenses in the lower levels of the IVZ section indicate that this hypothesis is unlikely. These findings support the interpretation that volcano-sedimentary material, deposited in the Rheic Ocean, was accreted to the deep crust during subduction, between ~340 and ~300 Ma, prior to regional high-temperature metamorphism.

Appendix A

Monazite textural setting

A.1.1 Included in garnet

Monazite included in garnet is only present in granulite facies samples. Two of the 66 total monazites in this study are included in garnet, AS06 monazite 6 and AS13 monazite 7. AS06 monazite 6 is a cluster of three rounded, anhedral grains ranging between 100 and 200 µm in diameter. AS13 monazite 7 is a subhedral, elongated grain 100 µm long with two significant embayments along one side of the grain and a rutile inclusion (Fig. A-1a).

A.1.2 Partially included in garnet

Monazite are classified as being partially included in garnet if more than 40% of the monazite grain boundaries are in contact with garnet. Two monazite grains from this study are partially included in garnet, and both are found in granulite facies sample AS13. The portion of AS13 monazite 2 that is surrounded by garnet has a sharp, euhedral morphology while the part of the grain exposed to the matrix is rounded. The shape of included portion of AS13 mirrors the contours of a round, 50 µm quartz inclusion in the garnet (Fig. A-1b). Monazites that are partially included in garnet range from 100 to 150 µm in diameter.

A.1.3 Included in biotite

All 17 monazites included in biotite are found in amphibolite facies metapelites, with 13 included grains in type 2 amphibolites. Monazite found in biotite are the most likely to have

inclusions, which are usually biotite with minor quartz and plagioclase. They range in diameter from 50 to 275µm, with an average of 100µm (Fig. A-1c). The long axis of included monazite grains is often oriented parallel to the foliation defined by the host biotite, suggesting that the two phases were growing simultaneously.

A.1.4 Partially included in biotite

Twelve monazites are partially included in biotite, with more than 40% of the monazite grain boundaries in contact with a biotite grain. (Fig. A-1d). Type 1 amphibolite sample MW04 features one of the partially included monazite grains, while Type 2 amphibolites host the remaining eleven. The subhedral to anhedral partially included grains are smaller than monazite that are entirely included in biotite, with diameters of 50-250 µm and an average of 80 µm. While some partially included monazite grains are oriented parallel to micaceous foliation, others intersect the foliation at angles between 30° and 50°.

A.1.5 Included in rutile

The 3 monazites that are included or partially included in rutile are restricted to AS07. The host rutile have coronas and veins of titanite, assumed to be a product of hydration and decreasing pressure associated with exhumation (Pearce and Wheeler 2014, Lucassen et al. 2011, Carswell and O'brien 1993). The monazite in rutile grains are large and rounded, with diameters of 200-300 µm (Fig. A-1e).

A.1.6 Matrix grains

Matrix grains are the most abundant type of grain in IVZ metapelites, with 31 of the 66 total monazites being hosted in the matrix. The few monazites (<5) that are included in quartz, alkali feldspar and plagioclase are included in the 'matrix grain' classification. Matrix monazite are anhedral to subhedral, and host inclusions of predominately quartz and plagioclase, with less common biotite (Fig. A-1f) Their diameter varies widely between 30-300 µm, with an average grain size of 100 µm.

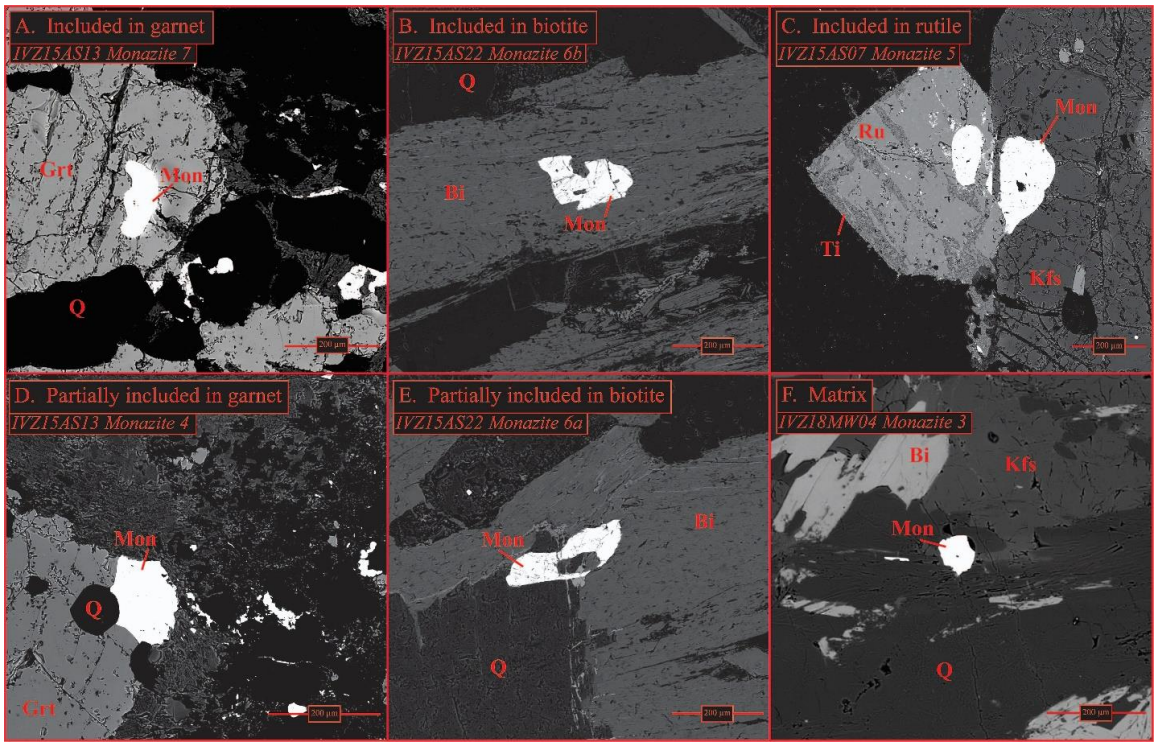

Figure A-1. Backscattered electron (BSE) images showing of textural settings of IVZ monazites.

Appendix B

Rare earth element zoning in monazite

Zoning in light rare earth elements (LREE) is uncommon in IVZ monazite. Of the 39 monazites mapped, four displayed zoning in LREE, and only one grain had an area where LREEs were significantly more enriched than the rest of the mineral. The following classifications are based on zoning in heavy rare earth elements (HREE), as identified based on Y abundance X-ray maps. No zoning is present in BSE images of all monazite grains. The type of zoning pattern does not appear to be affected by the size of the monazite grain.

B.1.1 No zoning

Monazites with no spatial variation in REE concentration are found at all structural levels: of the 15 unzoned monazite grains, six are from granulite facies samples, one is from a type 1 amphibolite sample, and 8 are from type 2 amphibolite samples (Fig. B-1a). Unzoned monazites are enriched in REE compared to the surrounding grains.

B.1.2 Concentric zoning

Concentric zoning is only observed in samples from granulite facies sample AS13. Monazite grains with concentric zoning feature a HREE depleted core surrounded by a thin (~5 µm) band of enrichment, a depleted mantle and a patchy, partially enriched rim, as typified by AS13 monazite 3 and monazite 6 (Fig. B-1b). AS13 monazite 7 features similar configuration with alternating areas of HREE enrichment and depletion; instead of thin bands of enriched areas, it features patchy zones of enrichment with a depleted core and rim. Concentric zoning is found

in monazite that are fully included in garnet and in matrix grains. This subgroup is the only type to feature zoning in LREE. LREE zoning follows a similar concentric pattern, but LREEs are enriched in areas of the grain where HREE is depleted.

B.1.3 Patchy Y enrichment

Patchy Y enrichment is defined as small (2-7 µm) areas of HREE enrichment found throughout the entire grain (Fig. B-1c). Enriched patches are often concentrated near the rim of the monazite. Patchy Y enrichment is not present in granulite facies samples. The 3 type 1 amphibolite monazite grains have smaller, more widely scattered patches that have internal variation Y concentration, while the three type 2 amphibolites have sharp boundaries between zones and more uniform Y concentrations within enriched areas (Fig. B-2).

B.1.4 Y enriched rim

Monazite crystals demonstrating Y-enriched rims have a similar appearance to patchy Y enrichment grains, but with a distinct Y depleted core that is devoid of areas of Y enrichment. The concentration of Y in the rim is does not vary widely. Of the fourteen grains with Y enriched rims, nine have a wide rim that surround a well-defined, angular core, and five have rims of inconsistent thickness that pinch and swell in rounded nodules that extend towards core (Fig. B-3). Y enriched rims are present in both type 1 and type 2 amphibolite monazite grains, and structural position does not affect the consistency of the rim thickness.

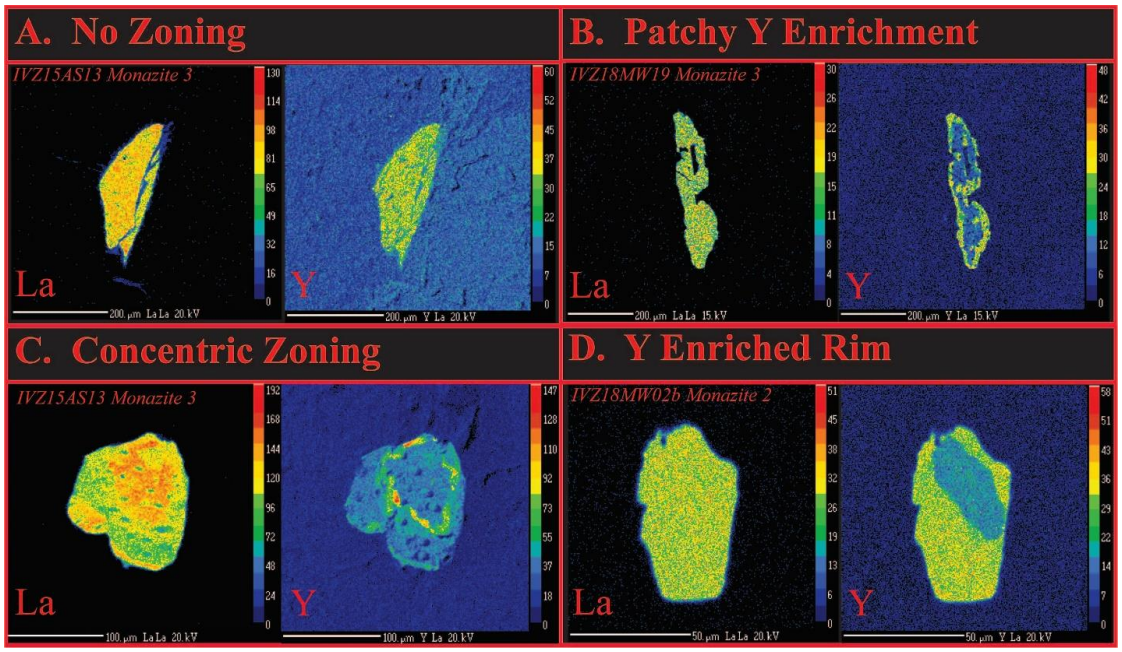

Figure B-1. X-Ray maps showing types of LREE and HREE zoning patterns. Color scale corresponds to counts during analysis.

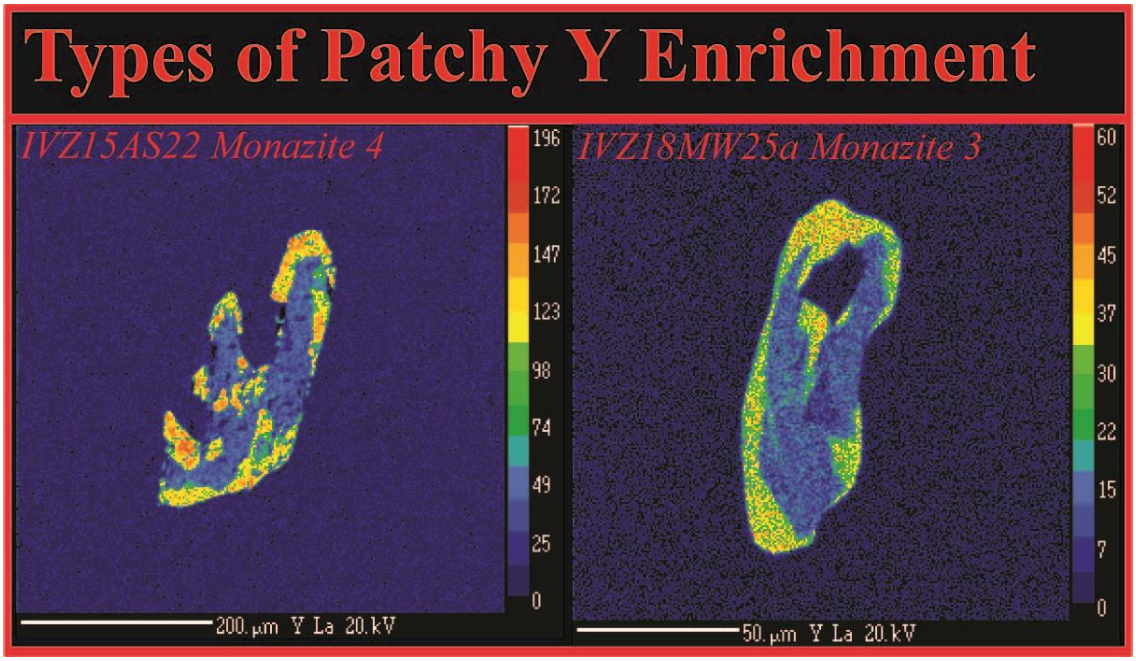

Figure B-2. X-Ray maps difference between patchy Y zoning patterns. Type 1 amphibolite monazite is shown on the left and features smaller, more widely scattered patches that have internal variation Y concentration, Type 2 amphibolite is shown on the right with sharp boundaries between zones and more uniform Y concentrations within enriched areas Color scale corresponds to counts during analysis.

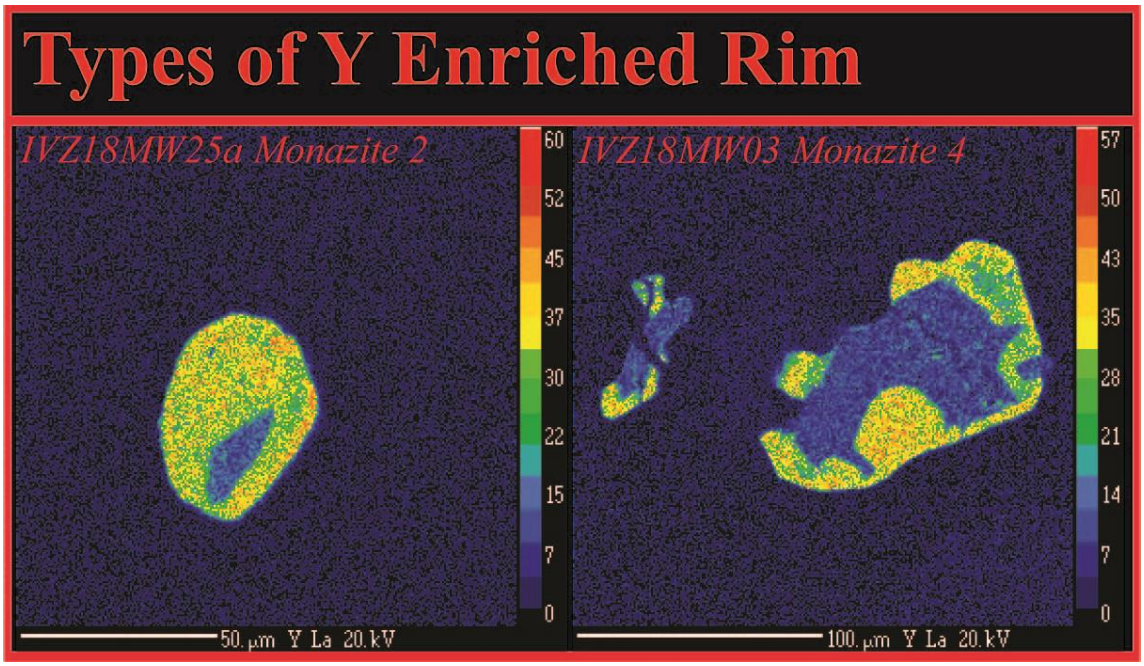

Figure B-3. X-Ray maps difference between types of Y enriched rims. Type 2 amphibolite monazite with wide rim that surrounds a well-defined, angular core is shown on the left, Type 1 amphibolite is shown on the right with a wide rim that surround a well-defined, angular core, and five have rims of inconsistent thickness that pinch and swell in rounded nodules that extend towards core. Color scale corresponds to counts during analysis.

REFERENCES

Aleinikoff, John N., William S. Schenck, Margaret O. Plank, LeeAnn Srogi, C. Mark Fanning, Sandra L. Kamo, and Howell Bosbyshell. 2006. "Deciphering igneous and metamorphic events in high-grade rocks of the Wilmington Complex, Delaware: Morphology, cathodoluminescence and backscattered electron zoning, and SHRIMP U-Pb geochronology of zircon and monazite." *GSA Bulletin* 118 (1-2):39-64. doi: 10.1130/b25659.1.

Allis, RG. 1981. "Continental underthrusting beneath the Southern Alps of New Zealand." *Geology* 9 (7):303-307.

Babist, J, MR Handy, M Konrad-Schmolke, and K Hammerschmidt. 2006. "Precollisional, multistage exhumation of subducted continental crust: The Sesia Zone, western Alps." *Tectonics* 25 (6).

Barboza, Scott A, and George W Bergantz. 2000. "Metamorphism and anatexis in the mafic complex contact aureole, Ivrea Zone, Northern Italy." *Journal of Petrology* 41 (8):1307-1327.

Barboza, Scott A, George W Bergantz, and Michael Brown. 1999. "Regional granulite facies metamorphism in the Ivrea zone: Is the Mafic Complex the smoking gun or a red herring?" *Geology* 27 (5):447-450.

Bea, Fernando, and Pilar Montero. 1999. "Behavior of accessory phases and redistribution of Zr, REE, Y, Th, and U during metamorphism and partial melting of metapelites in the lower crust: an example from the Kinzigite Formation of Ivrea-Verbano, NW Italy." *Geochimica et Cosmochimica Acta* 63 (7-8):1133-1153.

Behn, Mark D, and Peter B Kelemen. 2003. "Relationship between seismic P-wave velocity and the composition of anhydrous igneous and meta-igneous rocks." *Geochemistry, Geophysics, Geosystems* 4 (5).

Boriani, A, E Giobbi Origoni, A Borghi, and V Caironi. 1990. "The evolution of the “Serie dei Laghi”(Strona-Ceneri and Scisti dei Laghi): the upper component of the Ivrea-Verbano crustal section; Southern Alps, north Italy and Ticino, Switzerland." *Tectonophysics* 182 (1-2):103-118.

Boriani, Attilio, and Evelina Giobbi. 2004. "Does the basement of western southern Alps display a tilted section through the continental crust? A review and discussion." *Periodico di Mineralogia* 73 (2):5-22.

Boriani, Attilio, and Igor Villa. 1997. *Geochronology of regional metamorphism in the Ivrea-Verbano Zone and Serie dei Laghi, Italian Alps*. Vol. 77.

Brodie, K.H., E.H. Rutter, and P. Evans. 1992. "On the structure of the Ivrea-Verbano Zone (northern Italy) and its implications for present-day lower continental crust geometry." *Terra Nova* 4 (1):34-40. doi: 10.1111/j.1365-3121.1992.tb00448.x.

Brodie, KH, and EH Rutter. 1987. "Deep crustal extensional faulting in the Ivrea Zone of northern Italy." *Tectonophysics* 140 (2-4):193-212.

Brodie, KH, EH Rutter, and D Rex. 1989. "On the age of deep crustal extensional faulting in the Ivrea zone, northern Italy." *Geological Society, London, Special Publications* 45 (1):203-210.

Burke, Margaret M, and David M Fountain. 1990. "Seismic properties of rocks from an exposure of extended continental crust—new laboratory measurements from the Ivrea Zone." *Tectonophysics* 182 (1-2):119-146.

Carswell, DA, and PJ O'brien. 1993. "Thermobarometry and geotectonic significance of high-pressure granulites: examples from the Moldanubian Zone of the Bohemian Massif in Lower Austria." *Journal of Petrology* 34 (3):427-459.

Castro, Antonio, Katharina Vogt, and Taras Gerya. 2013. "Generation of new continental crust by sublithospheric silicic-magma relamination in arcs: a test of Taylor's andesite model." *Gondwana Research* 23 (4):1554-1566.

Christensen, Nikolas I, and Walter D Mooney. 1995. "Seismic velocity structure and composition of the continental crust: A global view." *Journal of Geophysical Research: Solid Earth* 100 (B6):9761-9788.

Coggon, R, and TJB Holland. 2002. "Mixing properties of phengitic micas and revised garnet-phengite thermobarometers." *Journal of Metamorphic Geology* 20 (7):683-696.

Davidson, Jon, Simon Turner, and Terry Plank. 2012. "Dy/Dy*: variations arising from mantle sources and petrogenetic processes." *Journal of Petrology* 54 (3):525-537.

de Capitani, Christian, and Thomas H Brown. 1987. "The computation of chemical equilibrium in complex systems containing non-ideal solutions." *Geochimica et Cosmochimica Acta* 51 (10):2639-2652.

de Capitani, Christian, and Konstantin Petrakakis. 2010. "The computation of equilibrium assemblage diagrams with Theriak/Domino software." *American Mineralogist* 95 (7):1006-1016.

DiPietro, JA. 2013. "Keys to the interpretation of geological history." *Landscape evolution in the United States*:3-95.

Ewing, Tanya A, Jörg Hermann, and Daniela Rubatto. 2013. "The robustness of the Zr-in-rutile and Ti-in-zircon thermometers during high-temperature metamorphism (Ivrea-Verbano Zone, northern Italy)." *Contributions to Mineralogy and Petrology* 165 (4):757-779.

Ewing, Tanya A, Daniela Rubatto, Marco Beltrando, and Jörg Hermann. 2015. "Constraints on the thermal evolution of the Adriatic margin during Jurassic continental break-up: U–Pb dating of rutile from the Ivrea–Verbano Zone, Italy." *Contributions to mineralogy and petrology* 169 (4):44.

Fountain, David M. 1976. "The Ivrea—Verbano and Strona-Ceneri Zones, Northern Italy: A cross-section of the continental crust—New evidence from seismic velocities of rock samples." *Tectonophysics* 33 (1):145-165. doi: https://doi.org/10.1016/0040-1951(76)90054-8.

Gerya, Taras V, and David A Yuen. 2003. "Rayleigh–Taylor instabilities from hydration and melting propel 'cold plumes' at subduction zones." *Earth and Planetary Science Letters* 212 (1-2):47-62.

Gordon, Stacia M, Samuel A Bowring, Donna L Whitney, Robert B Miller, and Noah McLean. 2010. "Time scales of metamorphism, deformation, and crustal melting in a continental arc, North Cascades USA." *Bulletin* 122 (7-8):1308-1330.

Green, Eleanor, Tim Holland, and Roger Powell. 2007. "An order-disorder model for omphacitic pyroxenes in the system jadeite-diopside-hedenbergite-acmite, with applications to eclogitic rocks." *American Mineralogist* 92 (7):1181-1189.

Guergouz, Celia, Laure Martin, Olivier Vanderhaeghe, Nicolas Thébaud, and Marco Fiorentini. 2018. "Zircon and monazite petrochronologic record of prolonged amphibolite to granulite facies metamorphism in the Ivrea-Verbano and Strona-Ceneri Zones, NW Italy." *Lithos* 308:1-18.

Hacker, Bradley, Andrew Kylander-Clark, and Robert Holder. 2019. "REE partitioning between monazite and garnet: Implications for petrochronology." *Journal of Metamorphic Geology* 37 (2):227-237.

Hacker, Bradley R, Peter B Kelemen, and Mark D Behn. 2011. "Differentiation of the continental crust by relamination." *Earth and Planetary Science Letters* 307 (3-4):501-516.

Hacker, Bradley R, Peter B Kelemen, and Mark D Behn. 2015. "Continental lower crust." *Annual Review of Earth and Planetary Sciences* 43:167-205.

Handy, MR, L Franz, F Heller, B Janott, and R Zurbriggen. 1999. "Multistage accretion and exhumation of the continental crust (Ivrea crustal section, Italy and Switzerland)." *Tectonics* 18 (6):1154-1177.

Henk, Andreas, Leander Franz, Stefan Teufel, and Onno Oncken. 1997. "Magmatic underplating, extension, and crustal reequilibration: Insights from a cross-section through the Ivrea Zone and Strona-Ceneri Zone, northern Italy." *The Journal of Geology* 105 (3):367-378.

Holland, Tim, Judy Baker, and Roger Powell. 1998. "Mixing properties and activity-composition relationships of chlorites in the system MgO-FeO-Al2O3-SiO2-H2O." *European Journal of Mineralogy*:395-406.

Holland, Tim, and Roger Powell. 2003. "Activity–composition relations for phases in petrological calculations: an asymmetric multicomponent formulation." *Contributions to Mineralogy and Petrology* 145 (4):492-501.

Holland, TJB, and RTJB Powell. 1998. "An internally consistent thermodynamic data set for phases of petrological interest." *Journal of metamorphic Geology* 16 (3):309-343.

Horstwood, Matthew SA, Gavin L Foster, Randall R Parrish, Stephen R Noble, and Geoff M Nowell. 2003. "Common-Pb corrected in situ U–Pb accessory mineral geochronology by LA-MC-ICP-MS." *Journal of Analytical Atomic Spectrometry* 18 (8):837-846.

Huerta, Audrey D, Leigh H Royden, and Kip V Hodges. 1998. "The thermal structure of collisional orogens as a response to accretion, erosion, and radiogenic heating." *Journal of Geophysical Research: Solid Earth* 103 (B7):15287-15302.

Hunziker, JC, and A Zingg. 1980. "Lower Paleozoic amphibolite to granulite facies metamorphism in the Ivrea Zone (southern Alps, northern Italy)." *Schweizerische Mineralogische und Petrographische Mitteilungen* 60:181-213.

Johnsson, Mark J. 1986. "Distribution of maximum burial temperatures across northern Appalachian Basin and implications for Carboniferous sedimentation patterns." *Geology* 14 (5):384-387.

Kelemen, Peter B., and Mark D. Behn. 2016. "Formation of lower continental crust by relamination of buoyant arc lavas and plutons." *Nature Geoscience* 9:197. doi: 10.1038/ngeo2662
https://www.nature.com/articles/ngeo2662#supplementary-information.

Kelly, Nigel M, Simon L Harley, and Andreas Möller. 2012. "Complexity in the behavior and recrystallization of monazite during high-T metamorphism and fluid infiltration." *Chemical geology* 322:192-208.

Kohn, Matthew J, and Frank S Spear. 1990. "Two new geobarometers for garnet amphibolites, with applications to southeastern Vermont." *American Mineralogist* 75 (1-2):89-96.

Kunz, Barbara E, Daniele Regis, and Martin Engi. 2018. "Zircon ages in granulite facies rocks: decoupling from geochemistry above 850° C?" *Contributions to Mineralogy and Petrology* 173 (3):26.

Kusbach, V, V Janoušek, Pavlina Hasalová, Karel Schulmann, CM Fanning, V Erban, and S Ulrich. 2015. "Importance of crustal relamination in origin of the orogenic mantle peridotite–high-pressure granulite association: example from the Náměšť Granulite Massif (Bohemian Massif, Czech Republic)." *Journal of the Geological Society* 172 (4):479-490.

Kylander-Clark, Andrew RC, Bradley R Hacker, and John M Cottle. 2013. "Laser-ablation split-stream ICP petrochronology." *Chemical Geology* 345:99-112.

Lakatos, Stephen, and Donald S Miller. 1983. "Fission-track analysis of apatite and zircon defines a burial depth of 4 to 7 km for lowermost Upper Devonian, Catskill Mountains, New York." *Geology* 11 (2):103-104.

Lanzirotti, A., and Gilbert N. Hanson. 1996. "Geochronology and geochemistry of multiple generations of monazite from the Wepawaug Schist, Connecticut, USA: implications for monazite stability in metamorphic rocks." *Contributions to Mineralogy and Petrology* 125 (4):332-340. doi: 10.1007/s004100050226.

Liou, JG, RY Zhang, and WG Ernst. 2007. "Very high-pressure orogenic garnet peridotites." *Proceedings of the National Academy of Sciences* 104 (22):9116-9121.

Liu, Jun, SR Bohlen, and WG Ernst. 1996. "Stability of hydrous phases in subducting oceanic crust." *Earth and Planetary Science Letters* 143 (1-4):161-171.

Lucassen, F, G Franz, P Dulski, RL Romer, and D Rhede. 2011. "Element and Sr isotope signatures of titanite as indicator of variable fluid composition in hydrated eclogite." *Lithos* 121 (1-4):12-24.

Mahar, Emma M, JM Baker, R Powell, TJB Holland, and N Howell. 1997. "The effect of Mn on mineral stability in metapelites." *Journal of Metamorphic Geology* 15 (2):223-238.

Mareschal, Jean-Claude, and Claude Jaupart. 2013. "Radiogenic heat production, thermal regime and evolution of continental crust." *Tectonophysics* 609:524-534.

Matzel, Jennifer EP, Samuel A Bowring, and Robert B Miller. 2004. "Protolith age of the Swakane Gneiss, North Cascades, Washington: Evidence of rapid underthrusting of sediments beneath an arc." *Tectonics* 23 (6).

Mazzucchelli, M., and F. Siena. 1986. "Geotectonic significance of the metabasites of the Kinzigitic Series, Ivrea-Verbano zone (Western Italian Alps)." *Tschermaks mineralogische und petrographische Mitteilungen* 35 (2):99-116. doi: 10.1007/bf01140842.

Mehnert, K. R. 1975. "The Ivrea Zone, a model of the deep crust." *N. Jb. Mineral. Abh.* 125:156-199.

Nahodilová, Radmila, Pavla Štípská, Roger Powell, Jan Košler, and Martin Racek. 2014. "High-Ti muscovite as a prograde relict in high pressure granulites with metamorphic Devonian zircon ages (Běstvina granulite body, Bohemian Massif): consequences for the relamination model of subducted crust." *Gondwana Research* 25 (2):630-648.

Nichols, Geoff T, Peter J Wyllie, and Charles R Stern. 1994. "Subduction zone melting of pelagic sediments constrained by melting experiments." *Nature* 371 (6500):785.

Palin, R. M., M. P. Searle, D. J. Waters, R. R. Parrish, N. M. W. Roberts, M. S. A. Horstwood, M.-W. Yeh, S.-L. Chung, and T. T. Anh. 2013. "A geochronological and petrological study of anatectic paragneiss and associated granite dykes from the Day Nui Con Voi metamorphic core complex, North Vietnam: constraints on the timing of metamorphism within the Red River shear zone." *Journal of Metamorphic Geology* 31 (4):359-387. doi: 10.1111/jmg.12025.

Paton, Chad, John Hellstrom, Bence Paul, Jon Woodhead, and Janet Hergt. 2011. "Iolite: Freeware for the visualisation and processing of mass spectrometric data." *Journal of Analytical Atomic Spectrometry* 26 (12):2508-2518.

Pearce, MA, and J Wheeler. 2014. "Microstructural and metamorphic constraints on the thermal evolution of the southern region of the Lewisian Gneiss Complex, NW Scotland." *Journal of Petrology* 55 (10):2043-2066.

Penniston-Dorland, Sarah C, Matthew J Kohn, and Craig E Manning. 2015. "The global range of subduction zone thermal structures from exhumed blueschists and eclogites: Rocks are hotter than models." *Earth and Planetary Science Letters* 428:243-254.

Peressini, Gabriella, JE Quick, Silvano Sinigoi, Albrecht W Hofmann, and M Fanning. 2007. "Duration of a large mafic intrusion and heat transfer in the lower crust: a SHRIMP U–Pb zircon study in the Ivrea–Verbano Zone (Western Alps, Italy)." *Journal of Petrology* 48 (6):1185-1218.

Pin, C. 1990. "Evolution of the lower crust in the Ivrea zone: a model based on isotopic and geochemical data." In *Granulites and crustal evolution*, 87-110. Springer.

Pyle, Joseph M, Frank S Spear, Roberta L Rudnick, and WILLIAM F McDONOUGH. 2001. "Monazite–xenotime–garnet equilibrium in metapelites and a new monazite–garnet thermometer." *Journal of Petrology* 42 (11):2083-2107.

Quick, James E, Silvano Sinigoi, and Adriano Mayer. 1994. "Emplacement dynamics of a large mafic intrusion in the lower crust, Ivrea-Verbano Zone, northern Italy." *Journal of Geophysical Research: Solid Earth* 99 (B11):21559-21573.

Quick, James E, Silvano Sinigoi, Arthur W Snoke, Thomas J Kalakay, Adriano Mayer, and Gabriella Peressini. 2003. "Geologic map of the southern Ivrea-Verbano Zone, northwestern Italy." *US Geological Survey*.

Quick, James E., Silvano Sinigoi, and Adriano Mayer. 1995. "Emplacement of mantle peridotite in the lower continental crust, Ivrea-Verbano zone, northwest Italy." *Geology* 23 (8):739-742. doi: 10.1130/0091-7613(1995)023<0739:eompit>2.3.co;2.

Redler, C., T. E. Johnson, R. W. White, and B. E. Kunz. 2012. "Phase equilibrium constraints on a deep crustal metamorphic field gradient: metapelitic rocks from the Ivrea Zone (NW Italy)." *Journal of Metamorphic Geology* 30 (3):235-254. doi: 10.1111/j.1525-1314.2011.00965.x.

Reichen, Laura E, and Joseph J Fahey. 1962. "improved method for the determination of FeO in rocks and minerals including garnet."

Rudnick, Roberta, and Shan Gao. 2014. "4.1 - Composition of the Continental Crust." In, 1-51.

Rudnick, Roberta L, and David M Fountain. 1995. "Nature and composition of the continental crust: a lower crustal perspective." *Reviews of geophysics* 33 (3):267-309.

Rudnick, Roberta L, and Shan Gao. 2003. "Composition of the continental crust." *Treatise on geochemistry* 3:659.

Rudnick, Roberta L, and Steven L Goldstein. 1990. "The Pb isotopic compositions of lower crustal xenoliths and the evolution of lower crustal Pb." *Earth and Planetary Science Letters* 98 (2):192-207.

Rutter, Ernest, Katharine Brodie, Tony James, and Luigi Burlini. 2007. "Large-scale folding in the upper part of the Ivrea-Verbano zone, NW Italy." *Journal of Structural Geology* 29 (1):1-17.

Sakaguchi, Arito. 1999. "Thermal maturity in the Shimanto accretionary prism, southwest Japan, with the thermal change of the subducting slab: fluid inclusion and vitrinite reflectance study." *Earth and Planetary Science Letters* 173 (1-2):61-74.

Sandiford, Mike, and Sandra McLaren. 2002. "Tectonic feedback and the ordering of heat producing elements within the continental lithosphere." *Earth and Planetary Science Letters* 204 (1-2):133-150.

Schaltegger, Urs, and Peter Brack. 2007. "Crustal-scale magmatic systems during intracontinental strike-slip tectonics: U, Pb and Hf isotopic constraints from Permian magmatic rocks of the Southern Alps." *International Journal of Earth Sciences* 96 (6):1131-1151.

Schmid, Rolf, and BJ Wood. 1976. "Phase relationships in granulitic metapelites from the Ivrea-Verbano Zone (Northern Italy)." *Contributions to Mineralogy and Petrology* 54 (4):255-279.

Schmid, SM. 1993. "Ivrea zone and adjacent southern Alpine basement." In *Pre-mesozoic geology in the Alps*, 567-583. Springer.

Schmid, SM, Andre Zingg, and M Handy. 1987. "The kinematics of movements along the Insubric Line and the emplacement of the Ivrea Zone." *Tectonophysics* 135 (1-3):47-66.

Schnetger, B. 1994. "Partial melting during the evolution of the amphibolite- to granulite-facies gneisses of the Ivrea Zone, northern Italy." *Chemical Geology* 113 (1):71-101. doi: https://doi.org/10.1016/0009-2541(94)90006-X.

Schulmann, Karel, Ondrej Lexa, Vojtěch Janoušek, Jean Marc Lardeaux, and Jean Bernard Edel. 2014. "Anatomy of a diffuse cryptic suture zone: an example from the Bohemian Massif, European Variscides." *Geology* 42 (4):275-278.

Sills, Jane D. 1984. "Granulite facies metamorphism in the Ivrea Zone, NW Italy." *Schweizerische Mineralogische und Petrographische Mitteilungen* 64 (1-2):169-191.

Sills, Jane D, and John Tarney. 1984. "Petrogenesis and tectonic significance of amphibolites interlayered with metasedimentary gneisses in the Ivrea Zone, Southern Alps, Northwest Italy." *Tectonophysics* 107 (3-4):187-206.

Sinigoi, S., J. E. Quick, A. Mayer, and J. Budahn. 1996. "Influence of stretching and density contrasts on the chemical evolution of continental magmas: an example from the Ivrea-Verbano Zone." *Contributions to Mineralogy and Petrology* 123 (3):238-250. doi: 10.1007/s004100050153.

Sinigoi, Silvano, James E Quick, Diane Clemens-Knott, Adriano Mayer, Gabbriella Demarchi, Maurizio Mazzucchelli, Luisa Negrini, and Giorgio Rivalenti. 1994. "Chemical evolution of a large mafic intrusion in the lower crust, Ivrea-Verbano Zone, northern Italy." *Journal of Geophysical Research: Solid Earth* 99 (B11):21575-21590.

Smith, Harold A., and Bruno J. Giletti. 1997. "Lead diffusion in monazite." *Geochimica et Cosmochimica Acta* 61 (5):1047-1055. doi: https://doi.org/10.1016/S0016-7037(96)00396-1.

Snoke, Arthur W, Thomas J Kalakay, James E Quick, and Silvano Sinigoi. 1999. "Development of a deep-crustal shear zone in response to syntectonic intrusion of mafic magma into the lower crust, Ivrea–Verbano zone, Italy." *Earth and Planetary Science Letters* 166 (1-2):31-45.

Spear, Frank S, and Joseph M Pyle. 2010. "Theoretical modeling of monazite growth in a low-Ca metapelite." *Chemical Geology* 273 (1-2):111-119.

Stacey, JS t, and 1JD Kramers. 1975. "Approximation of terrestrial lead isotope evolution by a two-stage model." *Earth and planetary science letters* 26 (2):207-221.

Syracuse, Ellen M, Peter E van Keken, and Geoffrey A Abers. 2010. "The global range of subduction zone thermal models." *Physics of the Earth and Planetary Interiors* 183 (1-2):73-90.

Tera, Fouad, and GJ Wasserburg. 1972. "U-Th-Pb systematics in three Apollo 14 basalts and the problem of initial Pb in lunar rocks." *Earth and Planetary Science Letters* 14 (3):281-304.

Tomascak, Paul B, Eirik J Krogstad, and Richard J Walker. 1996. "U-Pb monazite geochronology of granitic rocks from Maine: implications for late Paleozoic tectonics in the Northern Appalachians." *The Journal of Geology* 104 (2):185-195.

Vavra, G., Dieter Gebauer, Rolf Schmid, and William Compston. 1996. "Multiple zircon growth and recrystallization during polyphase Late Carboniferous to Triassic metamorphism in granulites of the Ivrea Zone (Southern Alps): an ion microprobe (SHRIMP) study." *Contributions to Mineralogy and Petrology* 122 (4):337-358. doi: 10.1007/s004100050132.

Vavra, Gerhard, and Urs Schaltegger. 1999. "Post-granulite facies monazite growth and rejuvenation during Permian to Lower Jurassic thermal and fluid events in the Ivrea Zone (Southern Alps)." *Contributions to Mineralogy and Petrology* 134 (4):405-414. doi: 10.1007/s004100050493.

Vavra, Gerhard, Rolf Schmid, and Dieter Gebauer. 1999. "Internal morphology, habit and U-Th-Pb microanalysis of amphibolite-to-granulite facies zircons: geochronology of the Ivrea Zone (Southern Alps)." *Contributions to Mineralogy and Petrology* 134 (4):380-404. doi: 10.1007/s004100050492.

Voshage, H., A. W. Hofmann, M. Mazzucchelli, G. Rivalenti, S. Sinigoi, I. Raczek, and G. Demarchi. 1990. "Isotopic evidence from the Ivrea Zone for a hybrid lower crust formed by magmatic underplating." *Nature* 347 (6295):731-736. doi: 10.1038/347731a0.

White, RW, R Powell, and TJB Holland. 2007. "Progress relating to calculation of partial melting equilibria for metapelites." *Journal of metamorphic Geology* 25 (5):511-527.

White, RW, R Powell, TJB Holland, and BA Worley. 2000. "The effect of TiO2 and Fe2O3 on metapelitic assemblages at greenschist and amphibolite facies conditions: mineral equilibria calculations in the system K2O-FeO-MgO-Al2O3-SiO2-H2O-TiO2-Fe2O3." *Journal of Metamorphic Geology* 18 (5):497-511.

White, RW, Roger Powell, and GL Clarke. 2002. "The interpretation of reaction textures in Fe-rich metapelitic granulites of the Musgrave Block, central Australia: constraints from mineral equilibria calculations in the system K2O–FeO–MgO–Al2O3–SiO2–H2O–TiO2–Fe2O3." *Journal of metamorphic Geology* 20 (1):41-55.

Xu, Qiang, Junmeng Zhao, Xiaohui Yuan, Hongbing Liu, and Shunping Pei. 2015. "Mapping crustal structure beneath southern Tibet: Seismic evidence for continental crustal underthrusting." *Gondwana Research* 27 (4):1487-1493.

Zhu, Chen, and Dimitri A Sverjensky. 1992. "F-Cl-OH partitioning between biotite and apatite." *Geochimica et Cosmochimica Acta* 56 (9):3435-3467.

Zingg, A. 1980. *Regional metamorphism in the Ivrea zone (southern Alps, N-Italy): field and microscopic investigations*. Vol. 60.

Zingg, A., M. R. Handy, J. C. Hunziker, and S. M. Schmid. 1990. "Tectonometamorphic history of the Ivrea Zone and its relationship to the crustal evolution of the Southern Alps." *Tectonophysics* 182 (1):169-192. doi: https://doi.org/10.1016/0040-1951(90)90349-D.